J. Fluid Mech. (1988), *vol.* 191, *pp.* 481–515
Printed in Great Britain

Nonlinear roll-up of externally excited free shear layers

By M. E. GOLDSTEIN† AND S. J. LEIB‡

†National Aeronautics and Space Administration, Lewis Research Center, Cleveland, OH 44135, USA

‡Case Western Reserve University, Cleveland, OH 44106, USA
and NASA Resident Research Associate

(Received 15 May 1987)

We consider the effects of strong critical-layer nonlinearity on the spatially growing instabilities of a shear layer between two parallel streams. A composite expansion technique is used to obtain a single formula that accounts for both shear-layer spreading and nonlinear critical-layer effects. Nonlinearity causes the instability to saturate well upstream of the linear neutral stability point. It also produces vorticity roll-up that cannot be predicted by linear theory.

1. Introduction

Numerous experiments involve external excitation of unsteady flows on unstable shear layers between two parallel streams. The resulting motion usually has harmonic time dependence, exhibits spatial growth in the downstream direction, and is well described – at least in its early stages – by linear, non-parallel-flow stability theory. This suggests that the initial instability-wave growth will eventually reverse (i.e. the linear wave will eventually decay) because of the shear-layer growth resulting from viscous diffusion effects. But experimentally observed shear layers usually 'roll-up' in the vicinity of the linear neutral stability point – suggesting that nonlinear effects become important there.

It should be possible to account for these effects by means of a local nonlinear solution that is valid somewhere in the vicinity of the linear neutral stability point. However, this solution should also be an appropriate continuation of the linear (weakly non-parallel) instability-wave solution into the downstream nonlinear region; which means that the two solutions should be required to match (in the matched asymptotic expansion sense) in some mutual overlap domain.

There are roughly two (not entirely independent) types of nonlinear theories. One of these – the so-called Stuart (1960) – Watson (1960) – Landau theory – is basically a multiple scales method that incorporates nonlinear effects into the lowest-order solution in order to eliminate secular terms in the higher-order solutions. These terms only appear when the solution remains at its neutral stability point over a sufficiently large streamwise distance. But this will only occur when the local Reynolds number is large enough to ensure that the mean flow remains parallel over this distance. The Reynolds number must also be small enough so that other stronger types of nonlinearity – to be discussed below – do not occur first. Huerre (1987) showed that it is impossible to simultaneously meet these requirements without introducing some type of artificial body force – which would defeat the whole purpose of the present analysis.

We are, therefore, forced to consider a stronger type of nonlinearity, namely the nonlinear critical-layer type. Nonlinear critical layers have been reviewed, in general, by Maslowe (1986); and by Stewartson (1981) for Rossby waves in particular. The reader is referred to these articles for details.

The early critical-layer analyses of Benney & Bergeron (1969), Davis (1969), and Haberman (1972) considered only the so-called equilibrium critical layers, in which the temporal development (or non-equilibrium) term does not explicitly appear in the critical-layer vorticity equation. Stewartson (1978), Warn & Warn (1978), Hickernell (1984), and others considered non-equilibrium or time-dependent critical layers for temporally growing (i.e. spatially periodic) Rossby waves.

Huerre & Scott's (1980) analysis – which is somewhat similar to the present analysis – shows that it is impossible to construct nonlinear equilibrium critical-layer solutions that match to a linear solution unless some sort of artificial body force is applied to the flow. This leaves us with the nonlinear, non-equilibrium-type critical layers considered by Stewartson (1978) and Warn & Warn (1978).

Robinson (1974) applied inviscid non-equilibrium, nonlinear, critical-layer theory to free-shear flows, but only considered the case where the deviation of the suitably normalized frequency from its neutral value was of the same order as the instability-wave amplitude ϵ and, therefore, could not (as will become clear below) match his solution onto the strictly linear instability-wave solution, which applies further upstream. Here we consider the case where the deviation of the local thickness Strouhal number (or normalized frequency) from the neutral value is $O(\epsilon^{\frac{1}{2}})$ and therefore large compared to the wave amplitude ϵ. The resulting lowest-order critical-layer vorticity equation contains both nonlinear and non-equilibrium terms and its solution can therefore be matched on to the upstream linear instability wave.

The critical layer develops gradually in space and has an $O(\epsilon^{\frac{1}{2}})$ effect on the growth rate of the linear instability wave (that continues to describe the dominant unsteady motion outside the critical layer), causing it to saturate at normalized frequencies well below the neutral frequency predicted by linear theory. It is worth noting that the Stuart–Watson (1960)-type interaction has a much smaller, $O(\epsilon^2)$, effect on the growth rate. An even more important result is that the predicted roll-up of the constant-vorticity lines is now substantially different from that predicted by linear theory which, in any case, should not be used for this purpose since the slope of the vorticity contours is assumed to be small there.

Since even the maximum linear growth rates are usually quite small – of the order of 0.1 or 0.2, depending on the normalization – we expect the critical-layer behaviour to extend relatively far upstream from the linear neutral point (perhaps even fairly close to the point where the local Strouhal number is half the neutral value, i.e. where the linear growth is maximum). This is shown very nicely in Michalke's (1964) figure 8 which is for temporally growing modes, but can be interpreted as a plot of the transverse vorticity distribution at various streamwise locations near the neutral stability point.

The problem is formulated in §2, where we show how the nonlinear critical-layer solution gradually evolves from the strictly linear, finite-growth-rate solution and that there exists an overlap domain where these two solutions can be matched. We calculate the flow in the near-neutral region just outside the critical layer in §3 by using an analysis that is in some respects similar to the one used by Huerre (1980, 1987) for a related problem involving a predominantly viscous critical layer.

We show that the growth of the externally imposed instability wave is ultimately

determined by the flow in the critical layer, which is analysed in §4. The vorticity transport, which includes lateral convection by the near-neutral instability mode, is governed by a linear first-order partial differential equation in this region but with one of its coefficients related to the yet undetermined amplitude of that instability mode. That amplitude is ultimately determined by matching the critical-layer solution to the outer near-neutral linear solution. This makes the overall problem nonlinear (and interactive) and it has to be solved numerically. The procedure, which involves a spectral decomposition of the solution, is described in §5.

Section 6 is concerned with the mean flow alteration produced by the instability wave. We show that the resulting mean flow change is $O(\epsilon^2)$ and is reflected in a corresponding change in the momentum thickness to that order. We derive a formula that relates this quantity to the mean-square instability-wave amplitude.

Overall instability-wave growth depends on both mean flow divergence and nonlinear effects in most of the relevant experiments. We therefore in §7 combine the present nonlinear solution with a slowly varying 'outer' solution to obtain a uniformly valid 'composite expansion' (Van Dyke 1975) that accounts for both effects in a single formula. It is our view that this approach is the only completely rational way to obtain such a formula.

The numerical results are discussed in §8. They show that the instability-wave growth rate can vanish well upstream of the linear neutral stability point but the final instability-wave amplitude is approached rather gradually (on the streamwise lengthscale of the inner region) through a successive series of decreasing-amplitude oscillations about the equilibrium position. The first few oscillations can be of rather large amplitude compared with the maximum instability-wave amplitude when the velocity change across the shear layer is small relative to the average velocity.

Speculations about the ultimate state of the critical layer are made with the aid of the non-interactive analytical solution of Stewartson (1978) and Warn & Warn (1978). Higher harmonics are generated in the outer flow at $O(\epsilon^{\frac{3}{2}})$, but only the first harmonic has significant amplitude there. Our predicted Reynolds-stress-induced shear-layer spread is shown to be in qualitative agreement with the experimental observations of Ho & Huang (1982). The numerical solution predicts vorticity roll-up that closely resembles experimental observation, with the formation of a particularly strong braid in the case where one of the streams has zero velocity.

2. Formulation

We are concerned with the two-dimensional flow in a nearly inviscid and incompressible shear layer between two parallel streams with nominally uniform velocities $U_1 > U_2$. The motion is governed by the vorticity equation

$$\frac{\partial \omega}{\partial t} + \partial(\omega, \psi) = \frac{1}{R}\nabla^2 \omega, \tag{2.1}$$

where

$$\nabla^2 \equiv \frac{\partial^2}{\partial y^2} + \frac{\partial^2}{\partial \xi^2}$$

is the Laplacian,

$$\omega = \nabla^2 \psi \tag{2.2}$$

is minus the dimensionless vorticity,

$$\partial(\omega, \psi) \equiv \frac{\partial \omega}{\partial \xi}\frac{\partial \psi}{\partial y} - \frac{\partial \omega}{\partial y}\frac{\partial \psi}{\partial \xi} \tag{2.3}$$

is the Jacobian with respect to ξ and y of ω and the stream function ψ. The latter is assumed to be non-dimensionalized by $\Delta\delta_0$, where

$$\Delta \equiv \tfrac{1}{2}(U_1 - U_2) \tag{2.4}$$

is a measure of the velocity difference across the shear layer and δ_0 denotes its characteristic thickness (to be specified more precisely below). We suppose that the time t has been normalized by δ_0/Δ and that the streamwise (in the U_1, U_2 direction) and transverse coordinates x and y, respectively, have been normalized by δ_0. Finally

$$\xi \equiv x - \bar{U}t \tag{2.5}$$

denotes the streamwise coordinate in a reference frame moving with the normalized average velocity

$$\bar{U} \equiv \frac{\tfrac{1}{2}(U_1 + U_2)}{\Delta} \tag{2.6}$$

of the two streams, and

$$R = \frac{\Delta\delta_0}{\nu}, \tag{2.7}$$

where ν is the kinematic viscosity, is a characteristic mean flow Reynolds number.

We require that the amplitude ϵ of the unsteady motion be small enough and the mean flow Reynolds number R be large enough to produce a nearly parallel mean flow, in which case the shear-layer width will initially increase only over the long (viscous) lengthscale

$$x_2 \equiv \frac{x}{R}. \tag{2.8}$$

The upstream unsteady motion is assumed to be small enough to be treated as a linear perturbation of this mean flow and we suppose that it consists of a time-harmonic spatially growing instability wave with Strouhal number S (based on Δ and δ_0). The associated unsteady flow will then be nearly inviscid with the dominant effect of viscosity being to change the local growth rate of the instability wave by causing the mean shear layer to thicken.

The unsteady flow can then be calculated by using weakly non-parallel stability theory, which amounts to using the multiple-scales method to correct the locally parallel flow approximation (i.e. the solution to Rayleigh's equation) to obtain a result that is uniformly valid over the long 'outer' lengthscale $x_2 = O(1)$, as was done, for example, by Crighton & Gaster (1976). The instability wave will then grow in amplitude with decreasing growth rate until it approaches neutral stability provided, of course, that its amplitude remains sufficiently small compared with the mean flow velocity (in the ξ-coordinate system) over most of the shear layer – as we now assume to be the case.

The unsteady instability-wave vorticity will then, as pointed out by Robinson (1974), develop a non-uniformity in the vicinity of the mean flow inflexion point. This non-uniformity does not affect the transverse mode shape and streamwise wavenumber of the linear instability wave – though, as shown below, it ultimately affects its growth rate and the higher-order terms in the asymptotic expansion which

it generates. Thus re-expanding the linear unsteady vorticity in terms of the small† 'parameter'

$$\sigma(x_2) \equiv S\frac{\delta(x_2)}{\delta_0} - S_0, \tag{2.9}$$

where S_0 denotes the neutral Strouhal number (as predicted by linear stability theory) and $\delta(x_2)$ denotes the local shear-layer thickness, will not yield a correct result in the region of non-uniformity, unless the y-coordinate is appropriately scaled with $\sigma(x_2)$ before this re-expansion is carried out.

The correct expression for the vorticity ω in this region, which turns out to have thickness $O(\sigma(x_2))$, is (see Robinson 1974 and Michalke 1964, figure 8 for temporally growing modes)

$$\psi_{yy} = \omega - \psi_{\xi\xi} = 1 - y^2 - \operatorname{Re}\epsilon A^\dagger\left(1 + \frac{2\sigma c_0}{y - \sigma c_0}\right) e^{i\alpha(\xi - \sigma c_0 t)} + o\left(\frac{y^2}{y - \sigma c_0}\right) \quad \text{as } \sigma \to 0; \quad \frac{y}{\sigma} = O(1), \tag{2.10}$$

where $\epsilon A^\dagger$ is the linear instability-wave amplitude, α is its complex wavenumber and $\sigma c_0 = c - \bar{U}$ is the deviation of its complex phase speed from its neutral value of $\bar{U}$.

Expanding this equation in powers of σ without accounting for the fact that $y/\sigma = O(1)$ would clearly lead to an incorrect result. Thus a different (boundary-layer type) expansion has to be used in the region where $y = O(\sigma)$, which we refer to as the 'linear' critical layer, or, following Robinson (1974), as the 'growth' critical layer.

Since the instability wave continues to grow as the neutral condition $\sigma(x_2) \to 0$ is approached, a point where the amplitude ϵ of the instability wave is $O(\sigma^2(x_2))$ must eventually be reached. Nonlinear effects will then be of the same order as instability-wave growth effects, and the critical-layer flow will then be governed by an equation of the type derived by Stewartson (1978) for time-dependent Rossby-wave critical layers.

Since the linear critical-layer expansion is a limiting form of this time-dependent, nonlinear critical-layer equation, the associated scaling $\sigma^2(x_2) = O(\epsilon)$ corresponds to a 'distinguished limit' for the 'inner' (nonlinear) expansion that matches onto the 'outer' (linear) expansion on the x_2-scale (where, as we have already indicated, the solution is uniformly valid in y and is given by the inviscid slowly varying approximation). The overlap domain corresponds to the linear critical-layer region indicated in figure 1, since the relevant flow can be found by re-expanding either the 'inner' (near-neutral) or the 'outer' (slowly diverging) solution.

Viscous effects can still be neglected in the inner (near-neutral) region provided we assume, as we shall now do, that $\sigma^3(x_2)R = O(\epsilon^{\frac{3}{2}}R) \gg 1$. In fact, we require that R satisfy the more stringent condition

$$\epsilon^2 R \gg 1, \tag{2.11}$$

so that viscous effects can be completely neglected in our analysis.

We take the origin of the (x, x_2)-coordinate system to be in this inner (near-neutral) region and let δ_0 now be the characteristic shear-layer thickness there (say twice the momentum thickness).

† Note that $\sigma(x_2)$ will be substantially constant over many shear-layer thicknesses and can therefore be treated as a constant for the present purposes.

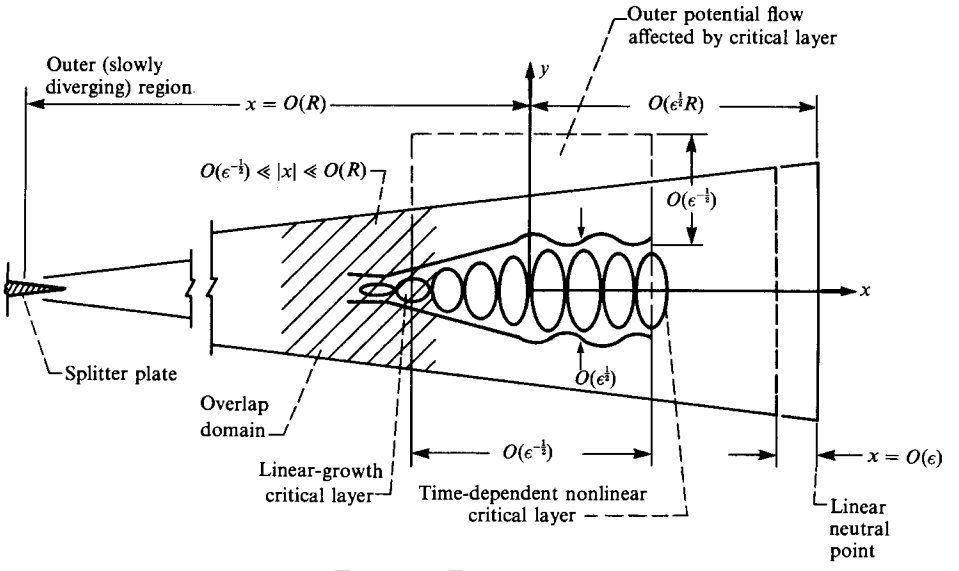

FIGURE 1. Flow structure.

3. Flow outside the critical layer

First consider the flow in the 'inner' (near-neutral) region where $\epsilon = O(\sigma^2(0))$. Since the linear instability wave is near its neutral point and has wavelength $O(\delta_0)$, our previous remarks suggest that the solution in the region $y = O(1)$ lying outside the critical layer will possess an expansion of the form

$$\psi = \psi_0(y) + \epsilon\psi_1 + \epsilon^{\frac{3}{2}}\psi_{\frac{3}{2}} + \epsilon^2\psi_2 + \epsilon^{\frac{5}{2}}\psi_{\frac{5}{2}} + O(\epsilon^3), \tag{3.1}$$

where the $\psi_{n/2}$ for $n = 2, 3, 4$, and 5 are functions of ξ and y and the 'slow' variables x_1 and t_1 to be defined subsequently.

Notice that $\psi_0(y)$ is a steady solution of the inviscid vorticity equation for any choice of the function ψ_0. The latter is determined by the slow development of the mean flow on the long viscous scale $x_2 = x/R$ and by the imposed upstream profile. We assume the latter to be such that

$$\psi_0 = \ln\cosh y \tag{3.2}$$

in the inner region, which closely corresponds to experimental observations and allows the analysis to be carried out explicitly.

The second term on the right-hand side of (3.1) represents the linear instability wave, which has an $O(1)$ wavelength relative to the ξ-scale and is near its neutral state, which corresponds to a neutral Strouhal number

$$S_0 = \bar{U} \tag{3.3}$$

for the profile (3.2). The small deviation, say $\epsilon^{\frac{1}{2}}S_1$, from this frequency, and the corresponding weak spatial amplification of the instability wave, can be accounted for by introducing the slow space and time variables

$$x_1 \equiv \epsilon^{\frac{1}{2}}x = \epsilon^{\frac{1}{2}}(\xi + \bar{U}t), \tag{3.4}$$

and

$$t_1 \equiv \epsilon^{\frac{1}{2}}t \tag{3.5}$$

in the laboratory (stationary) reference frame.

There is no need to introduce even slower (e.g. ϵx) scales as was done by Huerre (1980) since it is always possible to eliminate higher-order secularities in the present solution by exploiting arbitrarinesses in lower-order intermediate terms.

Substituting the expansion (3.1) into (2.1)–(2.4) and equating linear terms in ϵ to zero shows that

$$\mathscr{L}_0 \psi_1 = 0, \tag{3.6}$$

where we have put

$$\mathscr{L}_0 \equiv (U\nabla^2 - U'')\frac{\partial}{\partial \xi}, \tag{3.7}$$

with the primes denoting differentiation with respect to y, and

$$U = U(y) = \psi_0' = \tanh y \tag{3.8}$$

is the hyperbolic tangent mean velocity profile corresponding to the choice (3.2).

Equation (3.6) possesses the solution

$$\psi_1 = \operatorname{sech} y \operatorname{Re} A^{\dagger}(x_1)\, e^{i\zeta}, \tag{3.9}$$

where

$$\zeta \equiv \xi - S_1 t_1 = x - (\bar{U} + \epsilon^{\frac{1}{2}} S_1)\, t \tag{3.10}$$

denotes the streamwise coordinate in a reference frame moving with the actual 'phase velocity'

$$S \equiv \bar{U} + \epsilon^{\frac{1}{2}} S_1 = S_0 + \epsilon^{\frac{1}{2}} S_1 \tag{3.11}$$

of the mode (3.9), which differs from the average mean flow velocity $\bar{U}$ by the small amount $\epsilon^{\frac{1}{2}} S_1$.

The solution (3.9) clearly has harmonic time dependence with Strouhal number S in the laboratory reference frame, and can exhibit slow spatial growth through the 'slowly varying' amplitude function $A^{\dagger}(x_1)$, which will ultimately be determined by the second- and the third-order problems. This term is of exponential form in the strictly linear case where the amplitude of the instability wave is small relative to ϵ, and (3.9) then becomes the familiar exponentially growing eigenfunction of linear stability theory.

Our interest here is in time-periodic solutions of (2.1), and it is therefore appropriate to put

$$\psi_{n/2} = \operatorname{Re} \sum_{m=0}^{\infty} \Phi_{n/2}^{(m)}(y, x_1)\, e^{im\zeta} \quad \text{for } n = 3, 4, \ldots. \tag{3.12}$$

Then, since the slow time variable t_1 enters the solution only through ζ, it follows from (3.10) that

$$\frac{\partial}{\partial t_1} = -S_1 \frac{\partial}{\partial \zeta}. \tag{3.13}$$

The equations for the first few $\psi_{n/2}$ are

$$\mathscr{L}_0 \psi_{\frac{3}{2}} = -\mathscr{L}_1 \psi_1, \tag{3.14}$$

$$\mathscr{L}_0 \psi_2 = -\mathscr{L}_1 \psi_{\frac{3}{2}} - \Gamma_2 + \left(\frac{U''}{U}\right)' \psi_1 \psi_{1,\xi}, \tag{3.15}$$

$$\mathscr{L}_0 \psi_{\frac{5}{2}} = -\mathscr{L}_1 \psi_2 - \Gamma_{\frac{5}{2}} - \partial(\nabla^2 \psi_1, \psi_{\frac{3}{2}}) - \partial(\nabla^2 \psi_{\frac{3}{2}} + 2\psi_{1,x_1,\xi}, \psi_1) + \left(\frac{U''}{U}\right)' \psi_1 \psi_{1,x_1}, \tag{3.16}$$

where the subscripts denote partial differentiation with respect to the indicated variables – the partial derivatives with respect to x_1 being at constant t_1 and vice versa – and we have put

$$\mathscr{L}_1 \equiv \left[\frac{\partial}{\partial t_1}+(\bar{U}+U)\frac{\partial}{\partial x_1}\right]\nabla^2-\left(U''-2U\frac{\partial^2}{\partial \xi^2}\right)\frac{\partial}{\partial x_1}, \tag{3.17}$$

$$\Gamma_2 \equiv \left[(3U+2\bar{U})\frac{\partial}{\partial x_1}+2\frac{\partial}{\partial t_1}\right]\psi_1, \xi, x_1, \tag{3.18}$$

and, like $\Gamma_2, \Gamma_{\frac{5}{2}}$ involves no ζ-independent terms.

Substituting (3.9) and (3.12) into (3.14) shows that $\Phi_{\frac{3}{2}}^{(0)}$ is, at this stage, an arbitrary function of its arguments, and that $\Phi_{\frac{3}{2}}^{(1)}$, which accounts for the slow variation of the instability amplitude, satisfies Huerre's (1980) equation (3.7) with $\lambda = 0$, and is therefore given by his equation (3.11) with $\lambda = 0$. We reproduce it here in our notation for completeness:

$$\begin{aligned}\Phi_{\frac{3}{2}}^{(1)} = &-\mathrm{i}[(y\,\mathrm{sech}\,y+\sinh y)\ln|\tanh y|-\mathrm{sech}\,y\chi_2(\tanh y)]\left(\bar{U}\frac{\partial}{\partial x_1}-\mathrm{i}S_1\right)A^{\dagger}\\ &-\mathrm{i}\tanh y\sinh y\frac{\mathrm{d}A^{\dagger}}{\mathrm{d}x_1}+a_{\frac{3}{2}}^{(1)}\,\mathrm{sech}\,y+b_{\frac{3}{2}}^{(1)\pm}(y\,\mathrm{sech}\,y+\sinh y)\quad \text{for } y \gtrless 0.\end{aligned} \tag{3.19}$$

where

$$\chi_2(s) \equiv \int_0^s \frac{\tanh^{-1}(t)}{t}\mathrm{d}t,$$

$a_{\frac{3}{2}}^{(1)}$ and $b_{\frac{3}{2}}^{(1)\pm}$ are unknown functions of x_1, and the superscripts + and − refer, respectively, to the regions $y > 0$ and $y < 0$ since, as shown below, $\Phi_{\frac{3}{2}}^{(1)}$ must have a discontinuous first derivative across the critical layer in order to match the boundary-layer solution in this region.

As noted by Huerre (1980), $\Phi_{\frac{3}{2}}^{(1)}$ can only vanish at infinity if

$$b_{\frac{3}{2}}^{(1)+} = -b_{\frac{3}{2}}^{(1)-} = \mathrm{i}\frac{\mathrm{d}A^{\dagger}}{\mathrm{d}x_1},$$

which leads to the following relation between the amplitude $A^{\dagger}$ of the first-order solution (3.9) and the second-order 'jump' across the critical layer:

$$b_{\frac{3}{2}}^{(1)+}-b_{\frac{3}{2}}^{(1)-} = 2\mathrm{i}\frac{\mathrm{d}A^{\dagger}}{\mathrm{d}x_1}. \tag{3.20}$$

It is therefore necessary to consider the flow in the critical layer in order to determine $A^{\dagger}$. It is well known (e.g. Benney & Maslowe 1975; Robinson 1974) that $b_{\frac{3}{2}}^{(1)+}-b_{\frac{3}{2}}^{(1)-}$ is equal to

$$\pi\left(\bar{U}\frac{\partial}{\partial x_1}-\mathrm{i}S_1\right)A^{\dagger}$$

for a linear critical layer – corresponding to a logarithmic phase jump of $-\pi$ across that layer – so that

$$\frac{\mathrm{d}A^{\dagger}}{\mathrm{d}x_1} = -\tfrac{1}{2}S_1\kappa A^{\dagger},$$

where we have put

$$\kappa \equiv \kappa_{\mathrm{r}}+\mathrm{i}\kappa_{\mathrm{i}} \equiv \frac{\pi c_1}{S_1} \equiv \frac{\pi}{1+\frac{1}{2}\mathrm{i}\pi\bar{U}}. \tag{3.21}$$

We must therefore require that

$$A^{\dagger} \to a\, \mathrm{e}^{-\frac{1}{2}\kappa S_1 x_1} \quad \text{as } x_1 \to -\infty, \tag{3.22}$$

and it follows from (3.4) and (3.10) that $\epsilon^{\frac{1}{2}} c_1$ represents the first-order correction to the complex phase speed of the linear instability wave.

Higher harmonics of the $O(\epsilon^{\frac{3}{2}})$ solution satisfy the homogeneous equations

$$\mathrm{L}^{(n)} \Phi_{\frac{3}{2}}^{(n)} = 0 \quad \text{for } n = 2, 3, 4, \ldots, \tag{3.23}$$

where

$$\mathrm{L}^{(n)} \equiv \frac{\partial^2}{\partial y^2} - \left(n^2 + \frac{U''}{U} \right) \quad \text{for } n = 1, 2, 3, \ldots, \tag{3.24}$$

are the linear Rayleigh operators. Equations (3.23) possess the solution

$$\Phi_{\frac{3}{2}}^{(n)} = a_{\frac{3}{2}}^{(n)}(x_1)\, \mathrm{e}^{-n|y|} \left(1 + \frac{1}{n} \tanh |y| \right) \quad \text{for } n = 2, 3, 4, \ldots, \tag{3.25}$$

which clearly decay exponentially as $|y| \to \infty$ but have discontinuous first derivatives across $y = 0$. Discontinuities in the $\Phi_{\frac{3}{2}}^{(n)}$ $(n = 1, 2, 3, \ldots)$ themselves are precluded by the fact that solutions of the critical-layer vorticity equation cannot balance a transverse velocity jump at $O(\epsilon^{\frac{3}{2}})$. This implies continuity in pressure to the same order, as can be seen from the linearized streamwise momentum equation. The unknown $a_{\frac{3}{2}}^{(n)}$ will ultimately be determined by the flow in the critical layer, but it is first necessary to consider higher-order terms in the expansion (3.1) before calculating that flow.

Substituting (3.12) into (3.15), we find that the mean flow correction $\Phi_2^{(0)}$ is now an arbitrary function of its arguments, but the previously unknown mean flow correction $\Phi_{\frac{3}{2}}^{(0)}$ must now satisfy

$$\frac{\partial}{\partial x_1} \left[(U + \bar{U}) \frac{\partial^2}{\partial y^2} - U'' \right] \Phi_{\frac{3}{2}}^{(0)} = 0$$

in order to prevent the appearance of secular terms in ψ_2. It is sufficient to take

$$\Phi_{\frac{3}{2}}^{(0)} = \frac{U + \bar{U}}{\bar{U}} a_{\frac{3}{2}}^{(0)}(x_1), \tag{3.26}$$

and we shall eventually show that even this term must vanish.

The fundamental harmonic $\Phi_2^{(1)}$ satisfies

$$\mathrm{L}^{(1)} \Phi_2^{(1)} = F_2^{(1)}(y, x_1), \tag{3.27}$$

where $F_2^{(1)}$ is a complicated function of its arguments, which is written out in full in the Appendix. The higher harmonics satisfy

$$\mathrm{L}^{(n)} \Phi_2^{(n)} = \delta_{n,2} (A^{\dagger} \operatorname{sech}^2 y)^2 + \frac{2}{in} \left[\frac{\operatorname{sech}^2 y}{\tanh y} \left(\bar{U} \frac{\partial}{\partial x_1} - inS_1 \right) a_{\frac{3}{2}}^{(n)} + n^2 \frac{\mathrm{d} a_{\frac{3}{2}}^{(n)}}{\mathrm{d} x_1} \right]$$
$$\times\, \mathrm{e}^{-n|y|} \left(1 + \frac{1}{n} \tanh |y| \right) \quad \text{for } n = 2, 3, 4, \ldots. \tag{3.28}$$

Finally, we need to determine the unknown function $\Phi_2^{(0)}$. To this end we substitute (3.9), (3.12), and (3.19) into (3.16), to obtain Huerre's equation (3.17) with

$\lambda = 0$, so $\Phi_2^{(0)}$ must satisfy his equation (3.19) with $\lambda = 0$, which in the present notation becomes, upon neglecting an irrelevant function of y,

$$(\bar{U}+U)\,\Phi_{2y}^{(0)} - U'\Phi_2^{(0)} = -\tfrac{1}{2}|A^\dagger|^2\,\mathrm{sech}^4 y(\tfrac{1}{2}+\bar{U}\coth y) - P_{2,\infty}^{\pm}. \tag{3.29}$$

Integrating with respect to y yields

$$\begin{aligned}\Phi_2^{(0)} = &-(\bar{U}+\tanh y)\left\{\tfrac{1}{2}|A^\dagger|^2\left[\int_{\pm\infty}^{y}\mathrm{cosech}\, y\left(\frac{\mathrm{sech}^3 y}{\bar{U}+\tanh y}-\frac{1}{\bar{U}}\right)\mathrm{d}y\right.\right.\\ &+\frac{1}{\bar{U}}\ln|\tanh(\tfrac{1}{2}y)| - \bar{U}\ln\left|\frac{\bar{U}+\tanh y}{\bar{U}}\right|\Bigg]\\ &\left.+P_{2,\infty}^{\pm}\int_0^y\frac{\mathrm{d}y}{(\bar{U}+\tanh y)^2}-\frac{a_2^{(0)\pm}}{\bar{U}}\right\}+\tfrac{1}{4}|A^\dagger|^2[\bar{U}^2-1-(\bar{U}+\tanh y)^2],\end{aligned} \tag{3.30}$$

where the $P_{2,\infty}^{\pm}$ denote $O(\epsilon^2)$ mean pressure variations above/below the shear layer (Huerre 1980). $P_{2,\infty}^{-}$ must, of course, be set equal to zero when $\bar{U} = 1$.

Before analysing the flow in the critical layer, it is necessary to first determine the detailed asymptotic behaviour of the solution (3.1) in the neighbourhood of the origin $y = 0$. Fortunately, this can be done without obtaining complete solutions to the rather complicated equations (3.27) and (3.28) for the harmonics appearing in the $O(\epsilon^2)$ solution. Thus, retaining only the dominant terms in (A 1), (3.27) becomes

$$\begin{aligned}\mathrm{L}^{(1)}\Phi_2^{(1)} = 2\,\mathrm{sech}^3 y\coth y\Bigg[&\coth y\left(\bar{U}\frac{\partial}{\partial x_1}-\mathrm{i}S_1\right)^2 A^\dagger\\ &+\left(\bar{U}\frac{\partial}{\partial x_1}-\mathrm{i}S_1\right)\frac{\mathrm{d}A^\dagger}{\mathrm{d}x_1}-\mathrm{i}\left(\bar{U}\frac{\partial}{\partial x_1}-\mathrm{i}S_1\right)a_{\frac{3}{2}}^{(1)\pm}\Bigg]+O(\ln y)\quad\text{as } y\to 0.\end{aligned} \tag{3.31}$$

It therefore follows from the method of variation of parameters that

$$\Phi_2^{(1)} = -2\ln|y|\left(\bar{U}\frac{\partial}{\partial x_1}-\mathrm{i}S_1\right)^2 A^\dagger + a_2^{(1)\pm} + O(y\ln|y|)\quad\text{as } y\to 0, \tag{3.32}$$

where the $a_2^{(1)\pm}$ are arbitrary functions of x_1 associated with the complementary solutions of (3.31). In a similar way it follows from (3.28) that

$$\Phi_2^{(n)} = a_2^{(n)\pm} + O(y\ln|y|)\quad\text{as } y\to 0\quad\text{for } n = 2,3,4,\ldots. \tag{3.33}$$

4. The critical layer

We have already indicated that $\epsilon^{\frac{1}{2}}\delta_0$ is the appropriate transverse lengthscale in the critical layer. Introducing the scaled transverse coordinate

$$Y \equiv \frac{y}{\epsilon^{\frac{1}{2}}} \tag{4.1}$$

into the solutions (3.2), (3.9), (3.19), (3.25), (3.26), (3.30), (3.32), and (3.33), inserting

these into the expansion (3.1), re-expanding the result for small ϵ with $Y = O(1)$ held fixed, and retaining terms up to $O(\epsilon^2)$, yields

$$\begin{aligned}\psi = \mathrm{Re}\Big[&\epsilon(\tfrac{1}{2}Y^2 + A^\dagger \mathrm{e}^{\mathrm{i}\zeta}) + \epsilon^{\frac{3}{2}} \sum_{n=0}^{\infty} a_{\frac{3}{2}}^{(n)} \mathrm{e}^{\mathrm{i}n\zeta} \\ &- \epsilon^2 \ln \epsilon^{\frac{1}{2}} \Big[\tfrac{1}{2}|A^\dagger|^2 + 2\Big(\bar{U}\frac{\partial}{\partial x_1} - \mathrm{i}S_1\Big)\Big(\bar{U}\frac{\partial}{\partial x_1} - \mathrm{i}S_1 + \mathrm{i}Y\Big)A^\dagger \mathrm{e}^{\mathrm{i}\zeta}\Big] \\ &- \epsilon^2 \Big\{\tfrac{1}{2}Y^2(\tfrac{1}{6}Y^2 + A^\dagger \mathrm{e}^{\mathrm{i}\zeta}) + Y\Big[\mathrm{i}(\ln Y^2 - 1)\Big(\bar{U}\frac{\partial}{\partial x_1} - \mathrm{i}S_1\Big)A^\dagger \mathrm{e}^{\mathrm{i}\zeta} \\ &- a_{\frac{3}{2}}^{(0)}/\bar{U} - 2\sum_{n=1}^{\infty} b_{\frac{3}{2}}^{(n)\pm} \mathrm{e}^{\mathrm{i}n\zeta}\Big] + \Big[\ln Y^2\Big(\bar{U}\frac{\partial}{\partial x_1} - \mathrm{i}S_1\Big)A^\dagger \mathrm{e}^{\mathrm{i}\zeta} \\ &- \sum_{n=0}^{\infty} a_2^{(n)\pm} \mathrm{e}^{\mathrm{i}n\zeta}\Big] + \tfrac{1}{2}|A^\dagger|^2(I_\pm + \ln \tfrac{1}{2}|Y|)\Big\}\Big] + O(\epsilon^{\frac{5}{2}} \ln \epsilon), \end{aligned} \tag{4.2}$$

where we have put

$$b_{\frac{3}{2}}^{(n)\pm} \equiv \mp\tfrac{1}{2}\Big(n - \frac{1}{n}\Big)a_{\frac{3}{2}}^{(n)} \quad \text{for } n = 2, 3, 4, \ldots \tag{4.3}$$

and

$$I_\pm \equiv \bar{U}\int_{\pm\infty}^{0} \mathrm{cosech}\, y\Big(\frac{\mathrm{sech}^3 y}{\bar{U} + \tanh y} - \frac{1}{\bar{U}}\Big)\mathrm{d}y + \tfrac{1}{2}. \tag{4.4}$$

Equation (4.2) suggests that the critical-layer solution possess an expansion of the form

$$\Psi = \epsilon\Psi_0 + \epsilon^{\frac{3}{2}}\Psi_1 + \epsilon^2 \ln \epsilon^{\frac{1}{2}}\Psi_{2,L} + \epsilon^2\Psi_2 + \epsilon^{\frac{5}{2}}\Psi_3 + \ldots, \tag{4.5}$$

where the Ψ_n are functions of ζ, Y and x_1 only.

Substituting this into (2.1)–(2.3), equating to zero coefficients of like powers of ϵ, noting the upstream boundary condition (2.10) and the matching condition (4.2), we find that the first few terms in the expansion are

$$\Psi_0 = \tfrac{1}{2}Y^2 + \mathrm{Re}\, A^\dagger \mathrm{e}^{\mathrm{i}\zeta}, \tag{4.6}$$

$$\Psi_1 = \mathrm{Re} \sum_{n=0}^{\infty} a_{\frac{3}{2}}^{(n)} \mathrm{e}^{\mathrm{i}n\zeta}, \tag{4.7}$$

and

$$\Psi_{2,L} = -\tfrac{1}{2}|A^\dagger|^2 - 2\,\mathrm{Re}\Big(\bar{U}\frac{\partial}{\partial x_1} - \mathrm{i}S_1\Big)\Big(\bar{U}\frac{\partial}{\partial x_1} - \mathrm{i}S_1 + iY\Big)A^\dagger \mathrm{e}^{\mathrm{i}\zeta}. \tag{4.8}$$

Reinserting (4.5) into (2.1)–(2.3), equating coefficients of $\epsilon^{\frac{3}{2}}$ to zero, and using (3.13), and (4.6)–(4.8) now yields

$$\mathscr{L}^{(I)}\Omega_0 = 0, \tag{4.9}$$

$$\mathscr{L}^{(I)} \equiv \bar{U}\frac{\partial}{\partial x_1} + (Y - S_1)\frac{\partial}{\partial \xi} - \mathrm{Re}\,(\mathrm{i}A^\dagger \mathrm{e}^{\mathrm{i}\zeta})\frac{\partial}{\partial Y}, \tag{4.10}$$

where

$$\Omega_0 \equiv \Psi_{2Y,Y} + \Psi_{0\zeta,\zeta} = \Psi_{2Y,Y} - \mathrm{Re}\, A^\dagger \mathrm{e}^{\mathrm{i}\zeta}, \tag{4.11}$$

and $1 + \epsilon\Omega_0 + O(\epsilon^{\frac{3}{2}})$ is the critical-layer vorticity.

The method of characteristics shows that this equation possesses the solution

$$\Omega_0 = -Y^2 - 2\,\mathrm{Re}\,\mathrm{i}\int_{-\infty}^{x_1} A_0(\tilde{x})\,\mathrm{e}^{\mathrm{i}\zeta_S(\tilde{x})}\frac{\mathrm{d}\zeta_S(\tilde{x})}{\mathrm{d}\tilde{x}}\,\mathrm{d}\tilde{x}, \tag{4.12}$$

where we have put

$$A_0(x_1) \equiv A^\dagger(x_1)\,\mathrm{e}^{-\mathrm{i}S_1 x_1/\bar{U}}, \tag{4.13}$$

and $\zeta_S = \zeta_S(\tilde{x}\,|\,x_1, Y, \zeta)$ denotes the solution of the nonlinear characteristic equations

$$\bar{U}\frac{\mathrm{d}\zeta_S}{\mathrm{d}\tilde{x}}(\tilde{x}) = Y_S(\tilde{x}), \tag{4.14}$$

$$\bar{U}\frac{\mathrm{d}Y_S}{\mathrm{d}\tilde{x}}(\tilde{x}) = -\,\mathrm{Re}\,\mathrm{i}A_0(\tilde{x})\,\mathrm{e}^{\mathrm{i}\zeta_S(\tilde{x})}, \tag{4.15}$$

of (4.10), subject to the initial conditions

$$\zeta_S = \zeta + \frac{S_1}{\bar{U}}x_1, \quad Y_S = Y \quad \text{at } \tilde{x} = x_1. \tag{4.16}$$

Equations (3.21) and (3.22) show that $A^\dagger$, and hence A_0, vanish exponentially fast as $x_1 \to -\infty$, since $S_1 < 0$ upstream of the linear neutral stability point. Integrating by parts in (4.12) and using (4.13) and (4.16) therefore shows that

$$\Omega_0 = -Y^2 - 2\,\mathrm{Re}\,A^\dagger\,\mathrm{e}^{\mathrm{i}\zeta} + Q^\dagger, \tag{4.17}$$

where we have put

$$Q^\dagger \equiv 2\,\mathrm{Re}\int_{-\infty}^{x_1} A_0'(\tilde{x})\,\mathrm{e}^{\mathrm{i}\zeta_S(\tilde{x})}\,\mathrm{d}\tilde{x}. \tag{4.18}$$

Equations (4.14)–(4.16) show that

$$\zeta_S \to \zeta + \frac{S_1}{\bar{U}}x_1 + \frac{(\tilde{x}-x_1)\,Y}{\bar{U}} + (\text{exponentially small terms in } x_1 \text{ and } \tilde{x}) \quad \text{as } \tilde{x}, x_1 \to -\infty. \tag{4.19}$$

Inserting this along with (3.21) and (3.22) into (4.13), (4.17), and (4.18), using the result in (4.11) and noting that $\tilde{x} \leqslant x_1$, now shows that

$$\Psi_{2YY} = \Omega_0 - \Psi_{0\zeta\zeta} = -Y^2 - \mathrm{Re}\left(1 + \frac{2c_1}{Y-c_1}\right)a\,\mathrm{e}^{\mathrm{i}\zeta - \frac{1}{2}\pi c_1 x_1} + O(a^2\,\mathrm{e}^{2|c_1|x_1}) \quad \text{as } x_1 \to -\infty, \tag{4.20}$$

which, in view of (3.4), (3.5), (3.10), (3.21), (3.22), (4.1), and (4.5), clearly agrees with the linear critical-layer solution (2.10).

Integrating by parts in (4.18) (with respect to ζ_S) and using (3.21), (3.22), (4.13), (4.14), and (4.16) shows that

$$Q^\dagger = -\frac{2}{Y}\,\mathrm{Re}\,\mathrm{i}\left[\left(\bar{U}\frac{\partial}{\partial x_1} - \mathrm{i}S_1\right)A^\dagger\right]\mathrm{e}^{\mathrm{i}\zeta} + \frac{2}{Y^2}\,\mathrm{Re}\left[\left(\bar{U}\frac{\partial}{\partial x_1} - \mathrm{i}S_1\right)^2 A^\dagger\right]\mathrm{e}^{\mathrm{i}\zeta}$$
$$-2\,\mathrm{Re}\int_{-\infty}^{x_1}\left[\left(\frac{A_0''}{\zeta_S'^2}\right)' + \mathrm{i}\frac{A_0'\zeta_S''}{\zeta_S'^2}\right]\mathrm{e}^{\mathrm{i}\zeta_S}\,\mathrm{d}\tilde{x}. \tag{4.21}$$

Hence, using (4.14) and (4.15) to eliminate ζ_S'' and again integrating by parts yields

$$Q^\dagger = -\frac{2}{Y}\,\mathrm{Re}\,\mathrm{e}^{\mathrm{i}\zeta}\left(\mathrm{i}\bar{U}\frac{\partial}{\partial x_1} + S_1\right)A^\dagger - \frac{2}{Y^2}\left[\mathrm{Re}\,\mathrm{e}^{\mathrm{i}\zeta}\left(\mathrm{i}\bar{U}\frac{\partial}{\partial x_1} + S_1\right)^2 A^\dagger - \tfrac{1}{4}|A^\dagger|^2\right] + R_0, \tag{4.22}$$

where we have put

$$R_0 \equiv -2\int_{-\infty}^{x_1}\left\{\mathrm{Re}\left[\left(\frac{A_0''}{\zeta_S'^2}\right)'+\frac{A_0A_0'}{2(\bar{U}\zeta_S')^2}\,\mathrm{e}^{\mathrm{i}\zeta_S}\right]\mathrm{e}^{\mathrm{i}\zeta_S}+\frac{|A_0|^2}{4\bar{U}^2}\left(\frac{1}{\zeta_S'^2}\right)'\right\}\mathrm{d}\tilde{x}. \tag{4.23}$$

Since (4.14)–(4.16) ensure that $\zeta_S = O(Y)$ as $Y\to\infty$, these equations show that

$$R_0 = O(Y^{-3}) \quad \text{as } Y\to\infty. \tag{4.24}$$

Inserting (4.22) into (4.11) via (4.17) and integrating the result once with respect Y now shows that Ψ_2 matches the $O(\epsilon^2)$-terms in (4.2) if

$$2\,\mathrm{Re}\sum_{n=1}^{\infty}(b_{\frac{3}{2}}^{(n)+}-b_{\frac{3}{2}}^{(n)-})\,\mathrm{e}^{\mathrm{i}n\zeta} = \int_{-\infty}^{\infty}Q^{\dagger}\,\mathrm{d}Y. \tag{4.25}$$

where the improper integral $\int_{-\infty}^{\infty}Q^{\dagger}\,\mathrm{d}Y$ is defined in the usual way by

$$\int_{-\infty}^{\infty}Q^{\dagger}\,\mathrm{d}Y = \lim_{M\to\infty}\int_{-M}^{M}Q^{\dagger}\,\mathrm{d}Y.$$

It is now convenient to introduce the following normalized variables:

$$Q \equiv Q^{\dagger}/S_1^2\bar{U}, \tag{4.26}$$

$$A \equiv 4A^{\dagger}\,\mathrm{e}^{\mathrm{i}X_0}/\bar{U}^2S_1^2, \tag{4.27}$$

$$\eta \equiv -\frac{2(Y-S_1)}{S_1\bar{U}}, \tag{4.28}$$

$$X \equiv \zeta - X_0, \tag{4.29}$$

$$\bar{x} = -\tfrac{1}{2}S_1x_1 - x_0, \tag{4.30}$$

where

$$x_0 \equiv \frac{1}{\kappa_r}\ln\frac{(S_1\bar{U})^2}{4|a|} \tag{4.31}$$

and

$$X_0 \equiv -\kappa_{\mathrm{i}}x_0 - \arg a. \tag{4.32}$$

Then it follows from (3.20)–(3.22), (4.9), (4.12), (4.17), (4.20), and (4.25) that Q and A satisfy the scaled 'critical-layer vorticity equation':

$$\left[\frac{\partial}{\partial\bar{x}}+\eta\frac{\partial}{\partial X}-\mathrm{Re}\,(\mathrm{i}A\,\mathrm{e}^{\mathrm{i}X})\frac{\partial}{\partial\eta}\right]Q = \mathrm{Re}\,\mathrm{e}^{\mathrm{i}X}\left(\mathrm{i}A+\tfrac{1}{2}\bar{U}\frac{\mathrm{d}A}{\mathrm{d}\bar{x}}\right). \tag{4.33}$$

subject to the upstream boundary condition

$$\left.\begin{aligned} Q &\to \frac{1}{\pi}\,\mathrm{Re}\frac{\kappa A\,\mathrm{e}^{\mathrm{i}X}}{\eta-\mathrm{i}\kappa} \\ \text{and}\quad A &\to \mathrm{e}^{\kappa\bar{x}} \end{aligned}\right\} \quad \text{as } \bar{x}\to-\infty, \tag{4.34, 4.35}$$

along with the transverse jump condition

$$\frac{1}{\pi}\int_{-\infty}^{\infty}\int_{0}^{2\pi}\mathrm{e}^{-\mathrm{i}X}\,Q\,\mathrm{d}X\,\mathrm{d}\eta = \mathrm{i}\frac{\mathrm{d}A}{\mathrm{d}\bar{x}}, \tag{4.36}$$

which uniquely determines A and Q. Notice that $\bar{U}$ is the only parameter remaining in the problem.

It follows from (4.3) and (4.25), along with (4.26)–(4.32), that once Q is found, the harmonic amplitudes can be calculated from

$$a_{\frac{3}{2}}^{(n)} = \frac{S_1^3 \bar{U}^2}{4\pi\left(n-\frac{1}{n}\right)} e^{-inX_0} \int_0^{2\pi} e^{-inX} \int_{-\infty}^{\infty} Q \, d\eta \, dX \quad \text{for } n = 2, 3, 4, \ldots, \tag{4.37}$$

and that Q itself must satisfy the condition

$$\int_0^{2\pi} \int_{-\infty}^{\infty} Q \, d\eta \, dX = 0, \tag{4.38}$$

which we show to be the case in the next section.

5. Numerical computation

The nonlinear evolution equations (4.33)–(4.36) must be solved by numerical methods. Since Q is periodic in X, we expand it in a Fourier series

$$Q = \frac{1}{2} \sum_{n=-\infty}^{\infty} Q_n(\bar{x}, \eta) \, e^{inX}, \tag{5.1}$$

with

$$Q_{-n} = Q_n^* \tag{5.2}$$

(where the asterisk denotes the complex conjugate) to obtain

$$\left(\frac{\partial}{\partial \bar{x}} + in\eta\right) Q_n + \tfrac{1}{2}i \frac{\partial}{\partial \eta}(A^* Q_{n+1} - A Q_{n-1}) = \delta_{n,1}\left(iA + \tfrac{1}{2}\bar{U}\frac{dA}{d\bar{x}}\right), \quad \text{for } n = 0, 1, 2, 3, \ldots, \tag{5.3}$$

$$\int_{-\infty}^{\infty} Q_1 \, d\eta = i\frac{dA}{d\bar{x}}, \tag{5.4}$$

$$\left.\begin{aligned} Q_n &\to \frac{\kappa \delta_{n,1} A}{\pi(\eta - i\kappa)} \\ A &\to e^{\kappa \bar{x}} \end{aligned}\right\} \quad \text{as } \bar{x} \to -\infty. \tag{5.5}$$

We solved (5.3)–(5.5) numerically, using a procedure similar to the one used by Haynes (1985). Rather than mapping the infinite domain $-\infty < \eta < \infty$ into a finite region, Haynes simply solved his equation over a finite range, say $-M \leqslant \eta \leqslant M$, and used the asymptotic behaviour of Q as $\eta \to \pm\infty$ to obtain an accurate approximation to the integral in (5.4). In the present case it follows from (4.22), (4.24), and (4.26)–(4.29) that

$$Q_1 \to \frac{1}{\eta}\left(A - \tfrac{1}{2}i\bar{U}\frac{dA}{d\bar{x}}\right) + \frac{1}{\eta^2}\left(i\frac{dA}{d\bar{x}} + \tfrac{1}{2}\bar{U}\frac{d^2A}{d\bar{x}^2}\right) + O(\eta^{-4}) \quad \text{as } |\eta| \to \infty, \tag{5.6}$$

and consequently that (5.4) can be approximated by

$$\int_{-M}^{M} Q_1 \, d\eta = i\left(1 - \frac{2}{M}\right)\frac{dA}{d\bar{x}} - \frac{\bar{U}}{M}\frac{d^2A}{d\bar{x}^2} + O(M^{-3}). \tag{5.7}$$

Equation (5.3) was integrated forward in $\bar{x}$ beginning in the linear regime by a Hamming fourth-order predictor–corrector scheme (James, Smith & Wolford 1977) but with the $in\eta Q_n$ term always treated implicitly (as described by Haynes 1985).

Equations (5.5) provided the upstream conditions needed to start the calculation. Sixty Fourier components were used in the computation, but, in order to minimize aliasing, only the first 50 were used to actually calculate the vorticity via (5.1).

The transformation

$$\eta = \tilde{\eta} + \frac{10\tilde{\eta}^5}{(20)^4 + \tilde{\eta}^4} \tag{5.8}$$

was introduced into (5.3)–(5.5) and the computations done on a uniform mesh in the $\tilde{\eta}$-coordinate. This concentrated the mesh points near $\eta = 0$ where a higher resolution was required. The derivatives with respect to $\tilde{\eta}$ were replaced by a second-order central-difference formula, using the asymptotic expansion of Q to obtain values at the edges of the computational domain. Simpson's rule was used to evaluate the integral in (5.7).

We checked the calculated instability amplitude A with a completely independent computation based on the characteristic equations (4.14) and (4.15). The agreement was found to be excellent.

Equation (4.38) is equivalent to

$$\int_{-\infty}^{\infty} Q_0 \, \mathrm{d}\eta = 0. \tag{5.9}$$

But integrating (5.3) with $n = 0$ and using (5.2) and (5.6) shows that

$$\frac{\partial}{\partial \bar{x}} \int_{-\infty}^{\infty} Q_0 \, \mathrm{d}\eta = 0,$$

and since $Q_0 \to 0$ as $\bar{x} \to -\infty$ this implies that (5.9), and consequently also (4.38), are indeed satisfied.

Inserting (5.1) into (4.37) shows that the harmonic amplitudes in the outer flow are related to the critical-layer harmonic amplitudes Q_n by

$$a_{\frac{3}{2}}^{(n)} = \frac{S_1^3 \bar{U}^2 \, \mathrm{e}^{-\mathrm{i}nX_0}}{4\left(n - \frac{1}{n}\right)} \int_{-\infty}^{\infty} Q_n \, \mathrm{d}\eta, \quad n = 2, 3, 4, \ldots. \tag{5.10}$$

6. The change in mean flow

Equation (4.38) (or equivalently (5.9)) shows that there is no jump in tangential mean flow velocity across the critical layer to $O(\epsilon^2)$. The jump in this quantity is $O(\epsilon^{\frac{5}{2}})$, and integrating the relevant critical-layer vorticity equation shows that it is related to the jump in the $O(\epsilon^2)$ stream function by

$$\bar{U} \frac{\partial}{\partial x_1} \int_0^{2\pi} \int_{-\infty}^{\infty} \Psi_{3YY} \, \mathrm{d}Y \, \mathrm{d}\zeta = \frac{\partial}{\partial x_1} \int_0^{2\pi} \left[\Psi_2(\zeta, Y, x_1) - Y \frac{\partial}{\partial Y} \Psi_2(\zeta, Y, x_1) \right] \Bigg|_{-\infty}^{\infty} \mathrm{d}\zeta. \tag{6.1}$$

This latter quantity can be found from the outer boundary condition (4.2). It can also be found from the critical-layer vorticity equation (4.9), or equivalently (5.3) with $n = 0$. Integrating this latter equation twice and using (5.2), (5.4), and (5.6) yields

$$\frac{\partial}{\partial \bar{x}} \int_{-\infty}^{\infty} \mathrm{d}\eta \int_{-\infty}^{\eta} Q_0(\eta', \bar{x}) \, \mathrm{d}\eta' = \frac{\mathrm{d}(\frac{1}{2}|A|^2)}{\mathrm{d}\bar{x}},$$

or, equivalently

$$\int_{-\infty}^{\infty} \mathrm{d}\eta \int_{-\infty}^{\eta} Q_0(\eta', \bar{x}) \, \mathrm{d}\eta' = \tfrac{1}{2}|A|^2. \tag{6.2}$$

It therefore follows from (4.2), (4.11), (4.17), (4.26)–(4.29), and (5.1) that

$$S_1(\tfrac{1}{2}S_1\bar{U})^3\int_{-\infty}^{\infty}\mathrm{d}\eta\int_{-\infty}^{\eta}Q_0(\eta',\bar{x})\,\mathrm{d}\eta'=\frac{1}{2\pi}\int_0^{2\pi}\left[\Psi_2(\zeta,Y,x_1)-Y\frac{\partial}{\partial Y}\Psi_2(\zeta,Y,x_1)\right]\Bigg|_{-\infty}^{\infty}\mathrm{d}\zeta$$
$$=a_2^{(0)+}(x_1)-a_2^{(0)-}(x_1)-\tfrac{1}{2}|A^\dagger|\,(I_+-I_-)=\frac{1}{\bar{U}}|A^\dagger|^2. \quad (6.3)$$

This determines the jump in the slowly varying functions $a_2^{(0)\pm}$ that appear in the $O(\epsilon^2)$ mean flow correction (3.30).

The jump in the pressure function $P_{2\infty}^{\pm}$ is determined by the $O(\epsilon^{\frac{5}{2}})$ critical-layer vorticity equation. In fact it follows from (3.30) and (4.5) that

$$P_{2,\infty}^{+}-P_{2,\infty}^{-}-(a_2^{(0)+}-a_2^{(0)-})+\tfrac{1}{2}|A_0|^2\,(I_+-I_-)=-\frac{\bar{U}}{2\pi}\int_0^{2\pi}\int_{-\infty}^{\infty}\Psi_{3YY}\,\mathrm{d}Y\,\mathrm{d}\zeta. \quad (6.4)$$

Hence it follows from (6.1) and (6.3) that

$$\Delta P_{2,\infty}\equiv P_{2,\infty}^{+}-P_{2,\infty}^{-}=0. \quad (6.5)$$

Equations (3.1), (3.12), and (3.26) show that the change $\Delta\bar{\psi}$ in the mean stream function induced by the unsteady flow is

$$\Delta\bar{\psi}=\epsilon^{\frac{3}{2}}\frac{(\bar{U}+U)}{\bar{U}}a_{\frac{3}{2}}^{(0)}(x_1)+\epsilon^2\Phi_2^{(0)}+O(\epsilon^{\frac{5}{2}}). \quad (6.6)$$

$a_{\frac{3}{2}}^{(0)}$ is, at this stage, undetermined. It represents a simple displacement of the shear-layer centreline, since (6.6) can be combined with (3.8) to show that the mean shear-layer velocity, U_{M} say, is given by

$$U_{\mathrm{M}}\equiv\bar{U}+U+\frac{\partial}{\partial y}\Delta\bar{\psi}=\bar{U}+\tanh\left[y+\frac{\epsilon^{\frac{3}{2}}a_{\frac{3}{2}}^{(0)}(x_1)}{\bar{U}}\right]+O(\epsilon^2). \quad (6.7)$$

It is also worth noting that only the difference $P_{2,\infty}^{+}-P_{2,\infty}^{-}$ in the free-stream pressure variations (and not the individual pressures) is determined by the critical-layer flow (via (6.5)).

But since (6.6) and (3.30) show that

$$\Delta\bar{\psi}\to\epsilon^{\frac{3}{2}}\frac{(\bar{U}\pm1)}{\bar{U}}[a_{\frac{3}{2}}^{(0)}(x_1)+\epsilon^{\frac{1}{2}}a_2^{(0)\pm}(x_1)]$$
$$-\epsilon^2\left[\frac{P_{2,\infty}^{\pm}(x_1)}{\bar{U}\pm1}y+\text{function of }(x_1)\right]\quad\text{as } y\to\pm\infty\quad\text{when } \bar{U}\neq1, \quad (6.8)$$

and
$$\Delta\bar{\psi}\to0\quad\text{as } y\to-\infty\quad\text{when } \bar{U}=1, \quad (6.9)$$

the inviscid free-stream velocities, say $U_\infty^{\pm}$, $V_\infty^{\pm}$, induced by the mean shear-layer flow, must have expansions of the form

$$U_\infty^{\pm}=\bar{U}\pm1+\epsilon^2u_\infty^{\pm}(x_1,y_1)+O(\epsilon^{\frac{5}{2}}), \quad (6.10)$$

$$V_\infty^{\pm}=\epsilon^2v_\infty^{\pm}(x_1,y_1)+O(\epsilon^{\frac{5}{2}}), \quad (6.11)$$

where we have put
$$y_1\equiv\epsilon^{\frac{1}{2}}y, \quad (6.12)$$

since, as indicated in figure 1, the external potential flow must have equal streamwise and transverse lengthscales.

Matching with (6.8) shows that

$$u_\infty^\pm(x_1,0) = -\frac{P_{2,\infty}^\pm}{\bar{U}\pm 1}, \tag{6.13}$$

$$v_\infty^\pm(x_1,0) = -\frac{\bar{U}\pm 1}{\bar{U}}\frac{\mathrm{d}a_{\frac{3}{2}}^{(0)}}{\mathrm{d}x_1}, \tag{6.14}$$

when $U \neq 1$, and

$$u_\infty^-(x_1,0) = v_\infty^-(x_1,0) = 0 \quad \text{when } \bar{U} = 1. \tag{6.15}$$

But since $u_\infty^\pm, v_\infty^\pm$ are harmonic conjugate functions, their boundary values are related by the Hilbert transforms

$$v_\infty^\pm(x_1,0) = \mp\frac{1}{\pi}\int_{-\infty}^{\infty} \frac{u_\infty^\pm(\tilde{x}_1,0)}{\tilde{x}_1 - x_1}\mathrm{d}\tilde{x}_1, \tag{6.16}$$

where the bar indicates that the Cauchy principal value is to be taken. It now follows from (6.13) and (6.14) that

$$\int_{-\infty}^{\infty}\left[\frac{P_{2,\infty}^+(\tilde{x}_1)}{(\bar{U}+1)^2} + \frac{P_{2,\infty}^-(\tilde{x}_1)}{(\bar{U}-1)^2}\right]\frac{\mathrm{d}\tilde{x}_1}{\tilde{x}_1 - x_1} = 0 \quad \text{for } \bar{U} \neq 1,$$

which can only be satisfied if

$$\frac{P_{2,\infty}^+}{(\bar{U}+1)^2} = -\frac{P_{2,\infty}^-}{(\bar{U}-1)^2}. \tag{6.17}$$

Combining this with (6.5) shows that

$$P_{2,\infty}^\pm = 0. \tag{6.18}$$

Hence, it follows from (6.13)–(6.16) that

$$a_{\frac{3}{2}}^{(0)}(x_1) = 0, \tag{6.19}$$

and

$$U_\infty^\pm = \bar{U}\pm 1 + O(\epsilon^{\frac{5}{2}}). \tag{6.20}$$

It is difficult to give a truly satisfactory definition of momentum thickness, say Θ, for a shear layer, but it appears that the one often used by experimentalists (e.g. Oster & Wygnanski 1982) is

$$\Theta(U_\infty^+ - U_\infty^-)^2 \equiv \int_{-\infty}^{\infty} [U_{\mathrm{M}} - U_\infty^-(x_1,0)]\,[U_\infty^+(x_1,0) - U_{\mathrm{M}}]\,\mathrm{d}y. \tag{6.21}$$

Unfortunately, it is no longer possible to invoke a global conservation law to unambiguously relate this integral to shear-layer thickness, as can be done in the case of a boundary layer. Inserting (6.6), (6.7), (6.19), and (6.20) into the result shows that

$$4\Theta = \int_{-\infty}^{\infty}(1-U^2)\,\mathrm{d}y - 2\epsilon^2\int_{-\infty}^{\infty} U\frac{\partial \Phi_2^{(0)}}{\partial y}\mathrm{d}y. \tag{6.22}$$

But using (3.29) and (6.18) and integrating by parts shows that

$$-2\int_{-\infty}^{\infty} U\frac{\partial}{\partial y}\Phi_2^{(0)}\,\mathrm{d}y = (\bar{U}-1)\,\Phi_2^{(0)}(\infty) - (\bar{U}+1)\,\Phi_2^{(0)}(-\infty)$$
$$-\bar{U}[\Phi_2^{(0)}(0+) - \Phi_2^{(0)}(0-)] + \tfrac{1}{4}|A_0|^2\int_{-\infty}^{\infty}\mathrm{sech}^4 y\,\mathrm{d}y. \tag{6.23}$$

Inserting equation (3.30) and using (3.8), (4.4), (6.3), and (6.18) now shows that

$$\frac{4\Theta-2}{\epsilon^2|A_0|^2} = \bar{F}(\bar{U}) \equiv \tfrac{1}{3}-\frac{1}{\bar{U}^2}+\frac{\bar{U}^2-1}{2\bar{U}}\ln\left(\frac{\bar{U}+1}{\bar{U}-1}\right). \tag{6.24}$$

On using (4.30),

$$\frac{\Theta-\frac{1}{2}}{\frac{1}{2}\left(\frac{\epsilon^{\frac{1}{2}}S_1}{\bar{U}}\right)^4} = 8|A|^2(\tfrac{1}{2}\bar{U})^8\,\bar{F}(\bar{U}). \tag{6.25}$$

7. The composite expansion

Excitation experiments suggest that overall instability-wave growth is strongly dependent on both weakly non-parallel flow effects (due to viscous-shear-layer growth) and nonlinear effects such as those considered herein. There have, consequently, been a number of attempts to incorporate both effects into a single theory (e.g. Plaschko & Hussain 1984; Cohen 1985; Wygnanski & Petersen 1987) but as pointed out by Huerre (1980), viscous-shear-layer growth eventually produces an order-one deviation from the neutral state that invalidates the small-growth-rate assumption of any of the current nonlinear theories. This is because the non-parallel and nonlinear theories have different (spatial) regions of validity and, in our view, the only completely rational (i.e. self-consistent) way of incorporating both effects into a single formula is through the use of a 'composite expansion' (Van Dyke 1975) formed from the present, 'inner' (near-neutral) solution, say ψ_{inner}, and the slowly varying 'outer' solution, say ψ_{out}, which, as pointed out in §2, can be obtained by the method of multiple scales (Crighton & Gaster 1976) and can be written as

$$\psi_{\text{out}} = A_{\text{out}}(x_2)\,\Phi^{(1)}_{\text{out}}(y, x_2)\exp\left\{\mathrm{i}\left[\int_{x_e}^{x}\alpha(x_2)\,\mathrm{d}x - St\right]\right\}, \tag{7.1}$$

where $\Phi^{(1)}_{\text{out}}$ denotes the spatially growing eigensolution of Rayleigh's equation based on the local mean flow velocity at the streamwise position x_2 and normalized so that $\Phi^{(1)}_{\text{out}}(0, x_2) = 1, \alpha(x_2)$ denotes the corresponding complex eigenvalue, x_e is the streamwise location of the instability-wave source (usually the trailing edge of the splitter plate), and $A_{\text{out}}(x_2)$ is the slowly varying amplitude function determined by the elimination of secularity in an appropriate asymptotic expansion in powers of the slow divergence rate $1/R$.

We have, for the sake of concreteness, used a tanh mean velocity profile in our nonlinear analysis – though the principal results turn out to be nearly independent of the detailed profile shape. We suppose, therefore, for the sake of consistency, that the mean flow initial conditions† are adjusted to produce such a profile at the linear neutral stability point. However, the final formula ((7.9) below) should be more or less independent of the specific profile shape and should, therefore, apply for any starting flow.

Then

$$\Phi^{(1)}_{\text{out}}(y, x_2) \to \operatorname{sech} y \quad \text{as } x_2 \to 0, \tag{7.2}$$

since the origin of the coordinate system is assumed to lie in the inner nonlinear region. And since the small-growth-rate linear analyses of Monkewitz & Huerre (1982) and Robinson (1974) show that

$$\mathrm{i}\alpha \to \mathrm{i} - \frac{\epsilon^{\frac{1}{2}}S_1\,\pi}{2(1+\frac{1}{2}\mathrm{i}\bar{U}\pi)} = \mathrm{i} - \tfrac{1}{2}\epsilon^{\frac{1}{2}}S_1\,\kappa, \quad \text{as } x_2 \to 0, \tag{7.3}$$

† These can always be found by integrating the boundary-layer equation backwards.

with our normalization, where κ is defined by (3.21), it follows from (3.11) that

$$\psi_{\text{out}} \to \psi_{\text{o/i}} \equiv a \operatorname{sech} y \exp\left[-\tfrac{1}{2}S_1 \kappa x_1\right] \exp\left\{\mathrm{i}[x-(\bar{U}+\epsilon^{\frac{1}{2}}S_1)t]\right\} \quad \text{as } x_2 \to 0, \tag{7.4}$$

where we have put

$$a \equiv A_{\text{out}}(0) \exp\left[\mathrm{i}\int_{x_e}^{0} \alpha(x_2)\,\mathrm{d}x\right]. \tag{7.5}$$

The inner solution ψ_{inner} is given by (3.9). It therefore follows from (3.11) and (3.22) that

$$\psi_{\text{inner}} \to \psi_{\text{o/i}} \quad \text{as } x_1 \to -\infty.$$

$\psi_{\text{o/i}}$ therefore represents the common expansion of the inner solution (3.9), say ψ_{inner}, and ψ_{out} in their mutual overlap domain

$$\epsilon^{-\frac{1}{2}} \ll x \ll R. \tag{7.6}$$

Equations (3.9), (4.27), and (4.29)–(4.32) show that ψ_{inner} can be written as

$$\psi_{\text{inner}} = aA\, \mathrm{e}^{\sigma x_0} \operatorname{sech} y \exp\left\{\mathrm{i}[x-(\bar{U}+\epsilon^{\frac{1}{2}}S_1)t]\right\}. \tag{7.7}$$

Then (Van Dyke 1975)

$$\psi_{\text{comp}} \equiv \psi_{\text{out}}\psi_{\text{inner}}/\psi_{\text{o/i}} \tag{7.8}$$

is a uniformly valid composite expansion over the whole range of x and it follows from (7.1), (7.4), (7.7), and (7.8) that

$$\psi_{\text{comp}} = A_{\text{out}}(x_2)A(\bar{x})\,\mathrm{e}^{-\kappa\bar{x}}\Phi_{\text{out}}(y, x_2) \exp\left\{\mathrm{i}\left[\int_{x_e}^{x} \alpha(x_2)\,\mathrm{d}x - St\right]\right\}, \tag{7.9}$$

where the nonlinear effects are now accounted for by the 'amplification factor' $A\,\mathrm{e}^{-\kappa\bar{x}}$, which depends only on the average velocity ratio $\bar{U}$ and the shifted inner variable $\bar{x}$.

It follows from (4.30), (4.31), (7.2), and (7.5) that the latter is related to the original (unshifted) streamwise variable x by

$$\kappa_{\text{r}}\bar{x} = \ln\left[\frac{\left|A_{\text{out}}(0) \exp\left[\mathrm{i}\int_{x_e}^{x} \alpha(x_2)\,\mathrm{d}x\right]\right|}{(\tfrac{1}{2}S_1\bar{U})^2}\right]. \tag{7.10}$$

The argument of the logarithm is essentially the amplitude of the 'outer' (near-neutral) instability wave divided by the square of the deviation (see (2.9))

$$\epsilon^{\frac{1}{2}}S_1 = \sigma(x_2) = S\frac{\delta(x_2)}{\delta_0} - S_0$$

of the Strouhal number from the neutral Strouhal number $S_0 = \bar{U}$. We can allow the coordinate-system origin shift to occur naturally by reinserting the slow x_2 dependence into this equation to obtain

$$\kappa_{\text{r}}\bar{x} = \ln\left[\epsilon\frac{\left|A_{\text{out}}(x_2) \exp\left[\mathrm{i}\int_{x_e}^{x} \alpha(x_2)\,\mathrm{d}x\right]\right|}{(\tfrac{1}{2}\sigma(x_2)\bar{U})^2}\right], \tag{7.11}$$

which is of the same formal asymptotic order as (7.10) in the 'inner' (near-neutral) region (where $A(\bar{x})\,\mathrm{e}^{-\kappa\bar{x}}$ differs from unity), but allows the linear instability-wave growth itself to set the origin, $x = 0$, of the x-coordinate system and therefore the location of the 'inner' region.

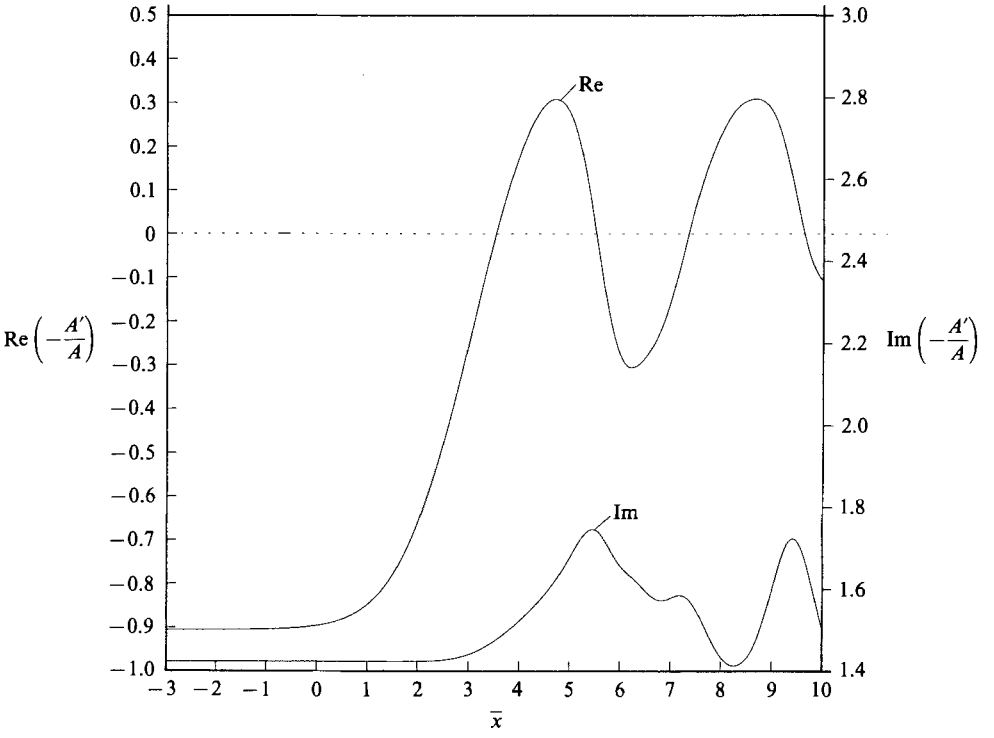

FIGURE 2. Scaled growth rate and wavenumber of 'fundamental' instability wave; $\bar{U} = 1.0$.

8. Numerical results and discussion

Goldstein, Durbin & Leib (1987) found that nonlinear critical-layer effects increase the stability of adverse-pressure-gradient boundary layers in the sense that they reduce instability-wave growth rates below those of linear theory. Similar effects are found in the present study – the most interesting result being that nonlinear effects reduce the growth rate to zero in a very short streamwise distance. In figure 2 the scaled growth rate $\mathrm{d}\ln|A|/\mathrm{d}\bar{x}$ of the 'outer' (near-neutral) instability wave (3.9) (see also (4.27)) is plotted as a function of the scaled (and shifted) streamwise coordinate $\bar{x}$ for the case $\bar{U} = 1$, where the low-speed stream has no velocity. It shows that $\mathrm{d}\ln|A|/\mathrm{d}\bar{x}$ follows the linear growth rate κ_r, until it rapidly decreases when $\bar{x}$ is about two. It then continues to oscillate about zero with what appears to be slowly decreasing amplitude. While we were unable to carry the numerical solution far enough to determine its ultimate asymptotic state, the results strongly suggest that

$$\frac{\mathrm{d}\ln|A|}{\mathrm{d}\bar{x}} \sim \frac{\cos(\gamma_1\bar{x}+\gamma_2)}{\bar{x}^{\gamma_0}} \quad \text{as } \bar{x}\to\infty, \tag{8.1}$$

where γ_0, γ_1, and γ_2 are real constants with $\gamma_0 \geqslant 0$.

The related Rossby-wave critical-layer solution of Stewartson (1978) and Warn & Warn (1978) (referred to in §1) also exhibits this behaviour. The latter solution corresponds to the case where critical-layer-induced 'outer' flow changes (in the Rayleigh region) cannot react back on the velocity field that advects the critical-layer vorticity. Their critical-layer vorticity equation was then linear and could therefore be solved analytically (in fact it was the same as our (4.33) with

$A = -1$ and Q replaced by $-Q$). Stewartson and Warn & Warn calculated the time evolution of Rossby-wave absorbtivity, which corresponds to the usual logarithmic phase jump across the critical layer, as does our scaled growth rate $\mathrm{d}\ln|A|/\mathrm{d}\bar{x}$. Their result, as reproduced in figure 1 of Killworth & McIntyre (1985), bears a remarkable resemblance to our figure 2. Killworth & McIntyre indicate that the oscillation amplitudes go to zero like $(\text{time})^{-2}$ as time $\to \infty$, which would correspond to $\gamma_0 = 2$ in (8.1). Our results suggest that γ_0 is smaller than this in the present case, but it is worth noting that the instability-wave amplitude $|A|$ will approach a definite value far downstream in the flow as long as γ_0 is strictly positive, and will continue to oscillate about a finite amplitude if $\gamma_0 = 0$. In either case the scaling used by Robinson (1974), which assumes the instability-wave amplitude $\epsilon A^{\dagger}$ to be large compared to the Strouhal-number deviation $\sigma^2(x_2)$ (and consequently that $A \gg 1$) is inappropriate even as an asymptotic limit of the present solution.

Stewartson's analytical solution also shows that the critical-layer vorticity itself does not tend to a steady-state limit, but continues to oscillate in the limit as $(\text{time}) \to \infty$ and appears to become increasingly dominated by the higher harmonics. He therefore concludes that even a small amount of viscosity will cause the critical layer to evolve into the Benney & Bergeron (1969) type, with constant 'cats-eyes' vorticity. Our feeling is that this still requires further verification. The present solution may not even tend to a steady state in the region outside the critical layer if it turns out that γ_0 is actually equal to zero.

Also plotted in figure 2 is the scaled wavenumber perturbation as a function of $\bar{x}$. It also follows the linear value κ_{i} until it begins to oscillate at the value of $\bar{x}$ for which the growth rate first goes to zero.

Figure 3 is a plot of the scaled instability-wave amplitude corresponding to the scaled growth rate plotted in figure 2. It shows the sudden deviation from linear growth in an even more dramatic fashion. The amplitude oscillations imply periodic reversal of energy transfer between the fluctuations and the mean flow, and possibly between the fluctuations themselves. By considering the Reynolds-stress changes that occur with nutating elliptic vortices, Browand & Ho (1983) came up with a simple kinematic explanation for this phenomenon. The reader is referred to Ho & Huerre (1984, p. 410) for details. Similar behaviour can be observed in the calculations of Benney & Maslowe (1975), Huerre (1977), and Miura & Sato (1978).

Figure 4 is a plot of the first few scaled harmonic amplitudes $|a_{\frac{1}{2}}^{(n)}|/S_1^3\bar{U}^2$, as calculated from (5.9). The figure shows that, while all outer-flow higher harmonics are generated by critical-layer nonlinearity, only the first ($n = 2$) harmonic has significant amplitude there.

Figures 5–7 are the analogues to 2–4, but are for the case where the scaled average velocity $\bar{U}$ is equal to three. They are similar to the previous figures, but the variations are now spread over much longer streamwise distances. Also, the scaled fundamental instability amplitude $|A|$ has a much smaller maximum value – about 0.2 as opposed to 7.5 – and the initial amplitudes of the downstream oscillations of $|A|$ are now significant fractions of its maximum value.

Figure 8 is a plot of the scaled momentum thickness change $(\Theta - \frac{1}{2})/\frac{1}{2}(\epsilon^{\frac{1}{2}}S_1/\bar{U})^4$, as given by (6.25), for the case $\bar{U} = 3.0$. It increases fairly gradually on the fast 'inner' scale $\bar{x}$, until it reaches a maximum value of about 14.5 at an $\bar{x}$ of about -9 and then very suddenly levels off and begins to decrease – because $|A|$ decreases. This variation in Θ would appear to be even more sudden when plotted against the slow outer variable x_2 on which the initial viscous-shear-layer growth takes place. This is

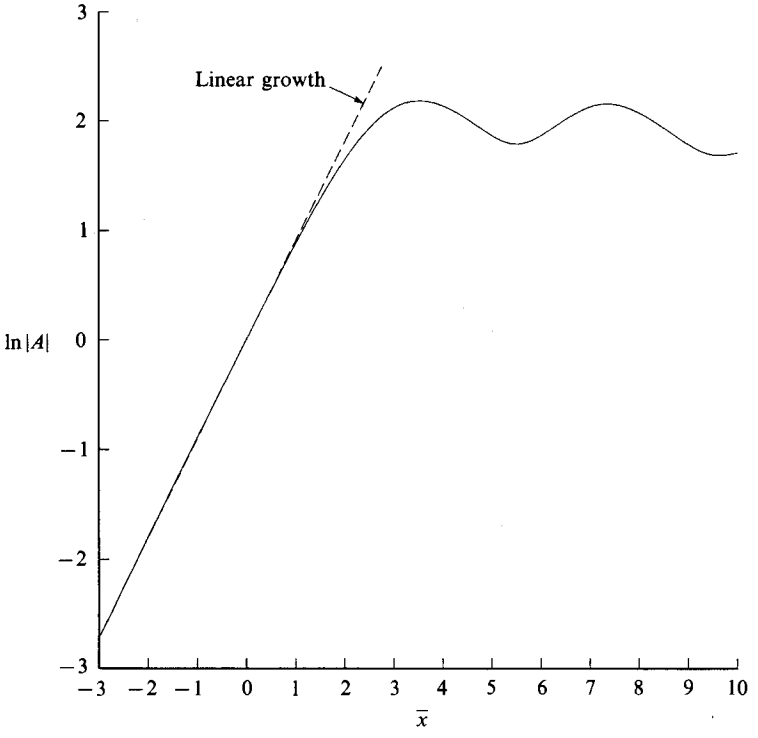

FIGURE 3. Scaled amplitude of 'fundamental' instability wave; $\bar{U} = 1.0$.

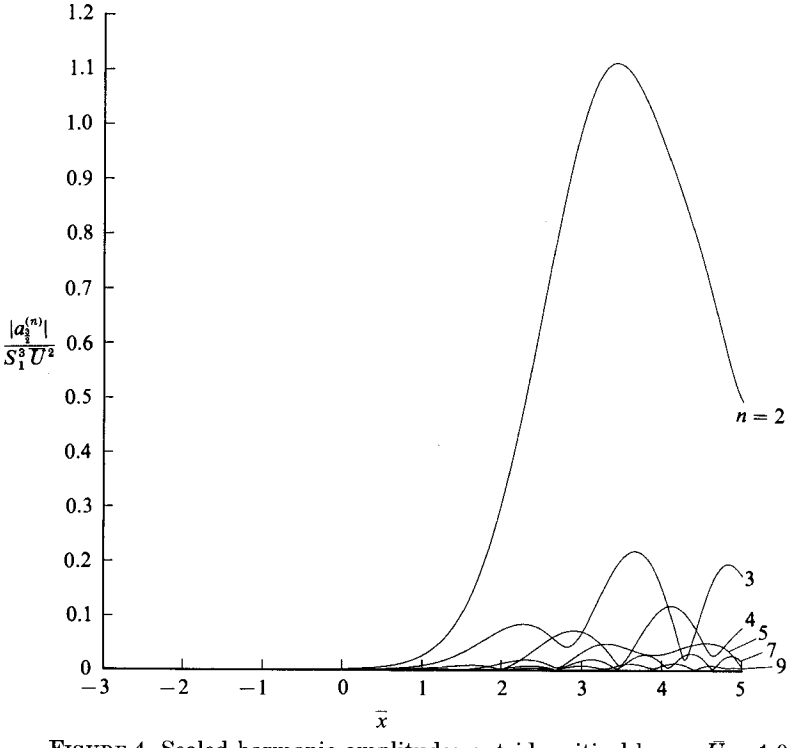

FIGURE 4. Scaled harmonic amplitudes outside critical layer; $\bar{U} = 1.0$.

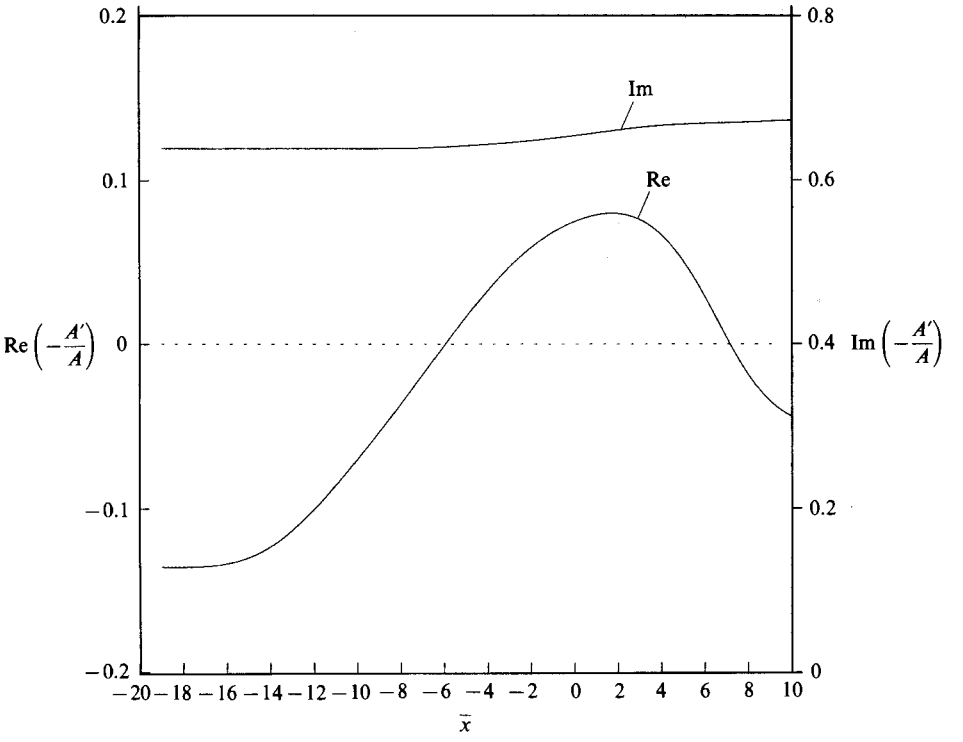

FIGURE 5. Scaled growth rate and wavenumber of 'fundamental' instability wave; $\bar{U} = 3.0$.

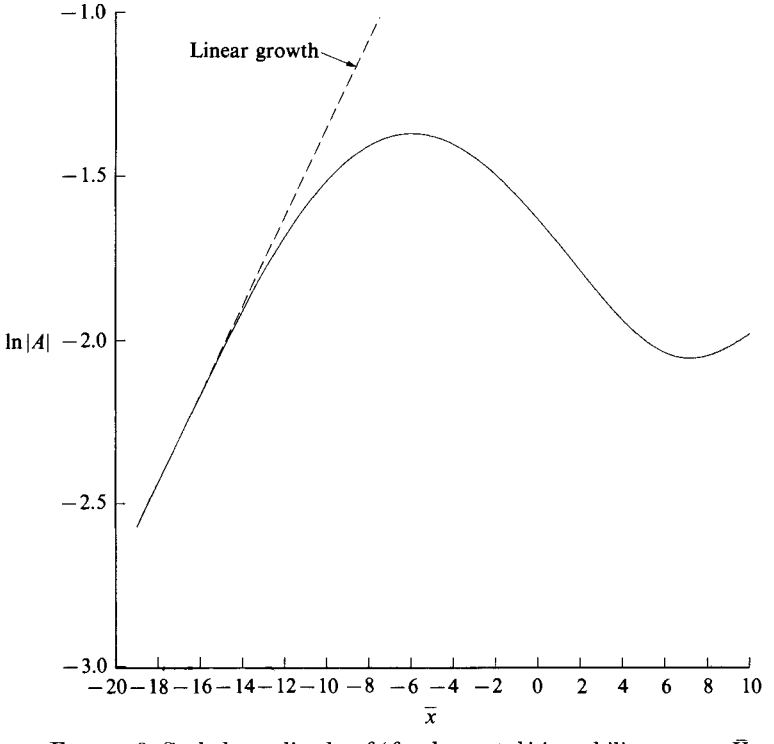

FIGURE 6. Scaled amplitude of 'fundamental' instability wave; $\bar{U} = 3.0$.

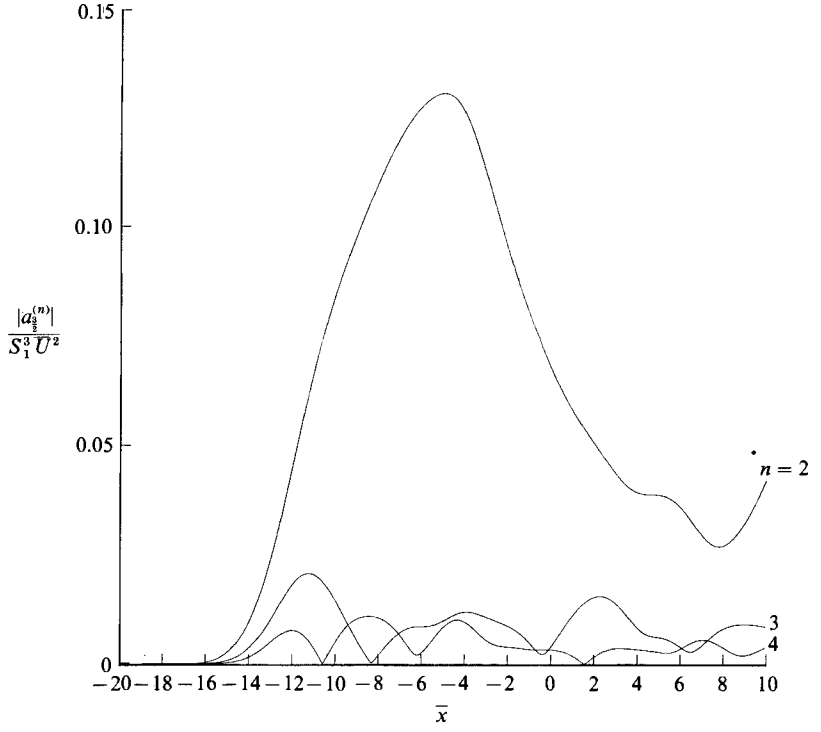

FIGURE 7. Scaled harmonic amplitudes outside critical layer; $\bar{U} = 3.0$.

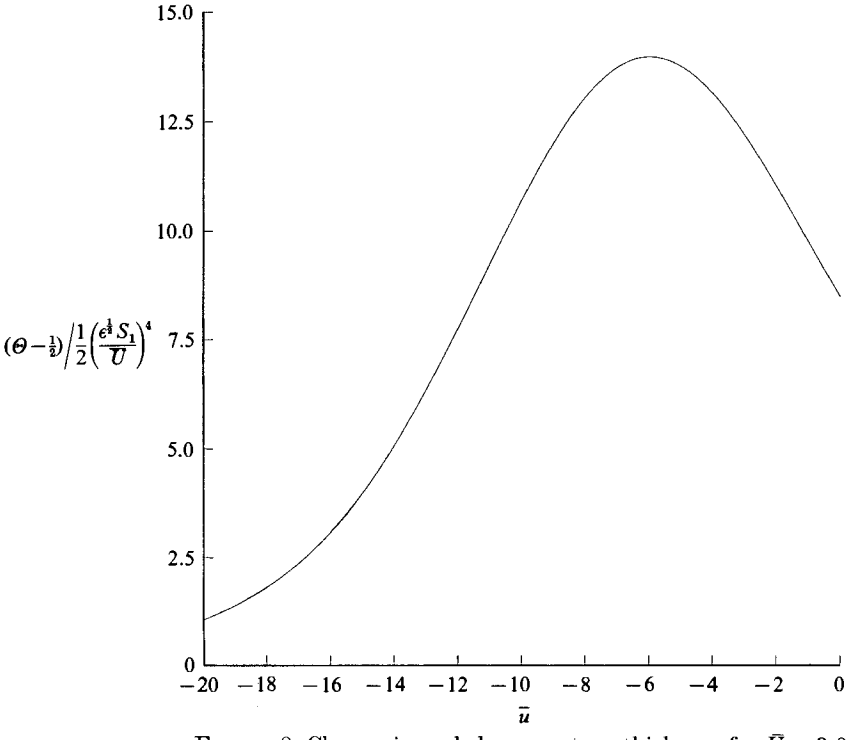

FIGURE 8. Change in scaled momentum thickness for $\bar{U} = 3.0$.

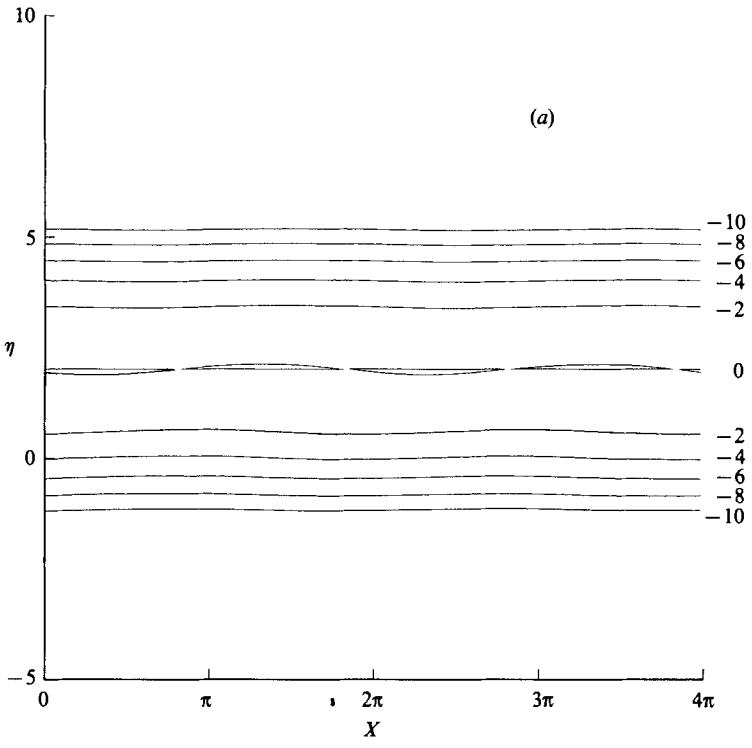

FIGURE 9(*a*). For caption see page 508.

consistent with the sudden change in shear-layer growth that was found to occur just upstream of the neutral stability point by Ho & Huang (1982). The quantity $(\epsilon^{\frac{1}{2}}S_1/\bar{U})$ in the denominator of (6.45) is the deviation of the frequency from the neutral frequency, divided by the neutral frequency at the position where nonlinear effects become important. We estimate that it should be about $\frac{1}{2}$ in the Ho & Huang experiment, so that (6.45) suggests that (instability-wave-induced shear-layer growth minus the viscous-shear-layer growth)/viscous-shear-layer growth ≈ 0.9, which appears to be consistent with Ho & Huang's observation for their case I. We expect that the large decrease in $\Theta - \frac{1}{2}$ beyond its maximum will be considerably reduced when a small amount of viscosity is included in the calculation.

Figure 9 is a plot of the constant-vorticity lines in the (X, η)-plane at various values of $\bar{x}$, for $\bar{U} = 1$. This figure shows that the vorticity exhibits the expected roll-up with downstream distance. The reader should note the especially strong braid that forms at $\bar{x} = 2.5$ and that roll-up occurs in the present analysis without significant mean flow divergence (Wygnanski & Petersen 1987, p. 206).

Standard computer routines for plotting contour lines tend to represent long, thin closed contours by series of small islands (as previously pointed out by Corcos & Sherman (1976), for example). The appearance of these islands in the $\Omega_0 = 0$ contour is probably attributable to this limitation, but some of the contour irregularity at the larger values of $\bar{x}$ is probably due to the inability of the numerical scheme to resolve small-scale details of the vorticity field.

For comparison we included figure 10 to show the downstream evolution of the vorticity contours predicted by the linear growth solution (4.20). It shows that the initial shearing of the constant-vorticity lines is well described by the linear theory

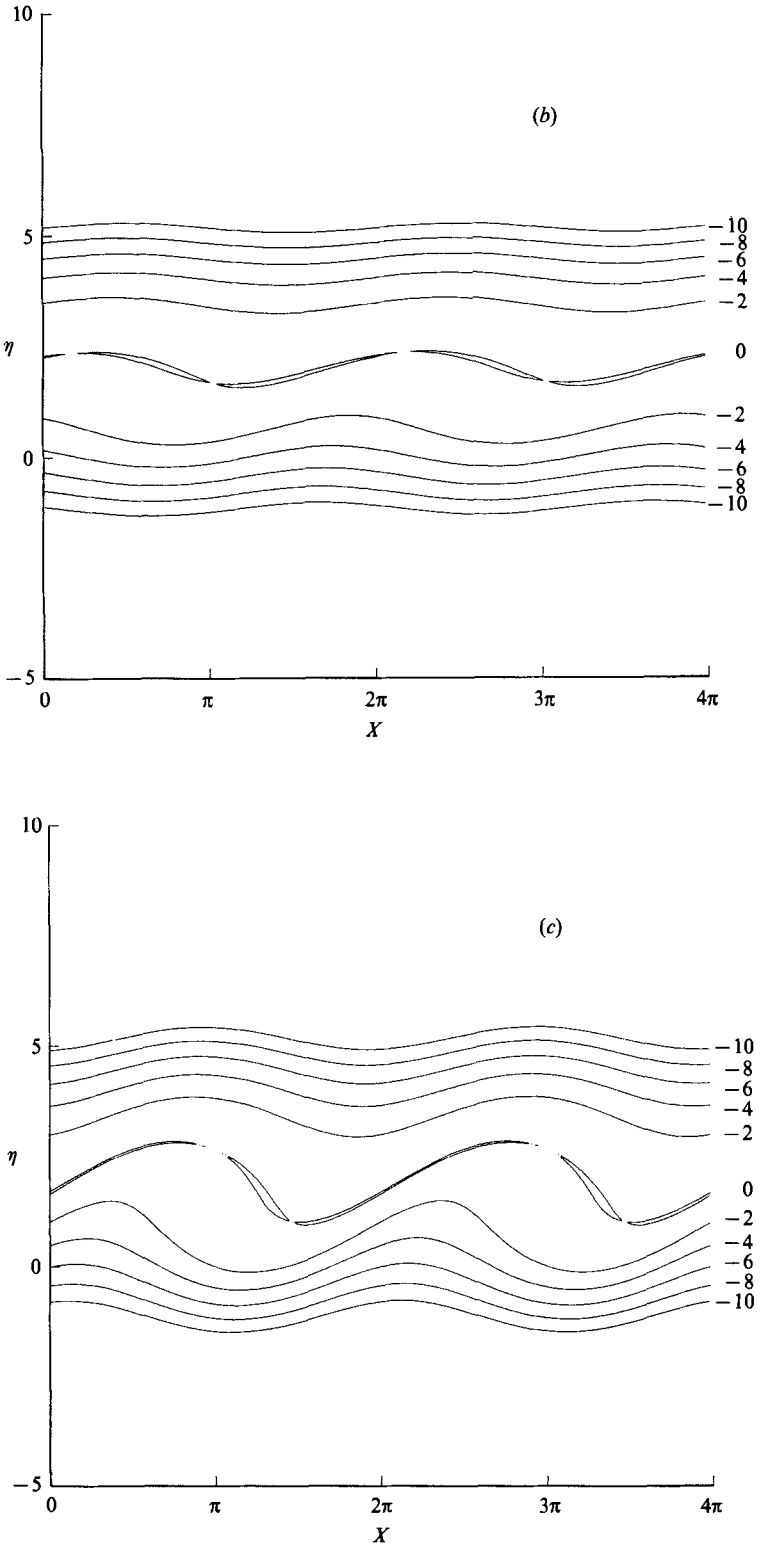

FIGURE 9(*b*, *c*). For caption see page 508.

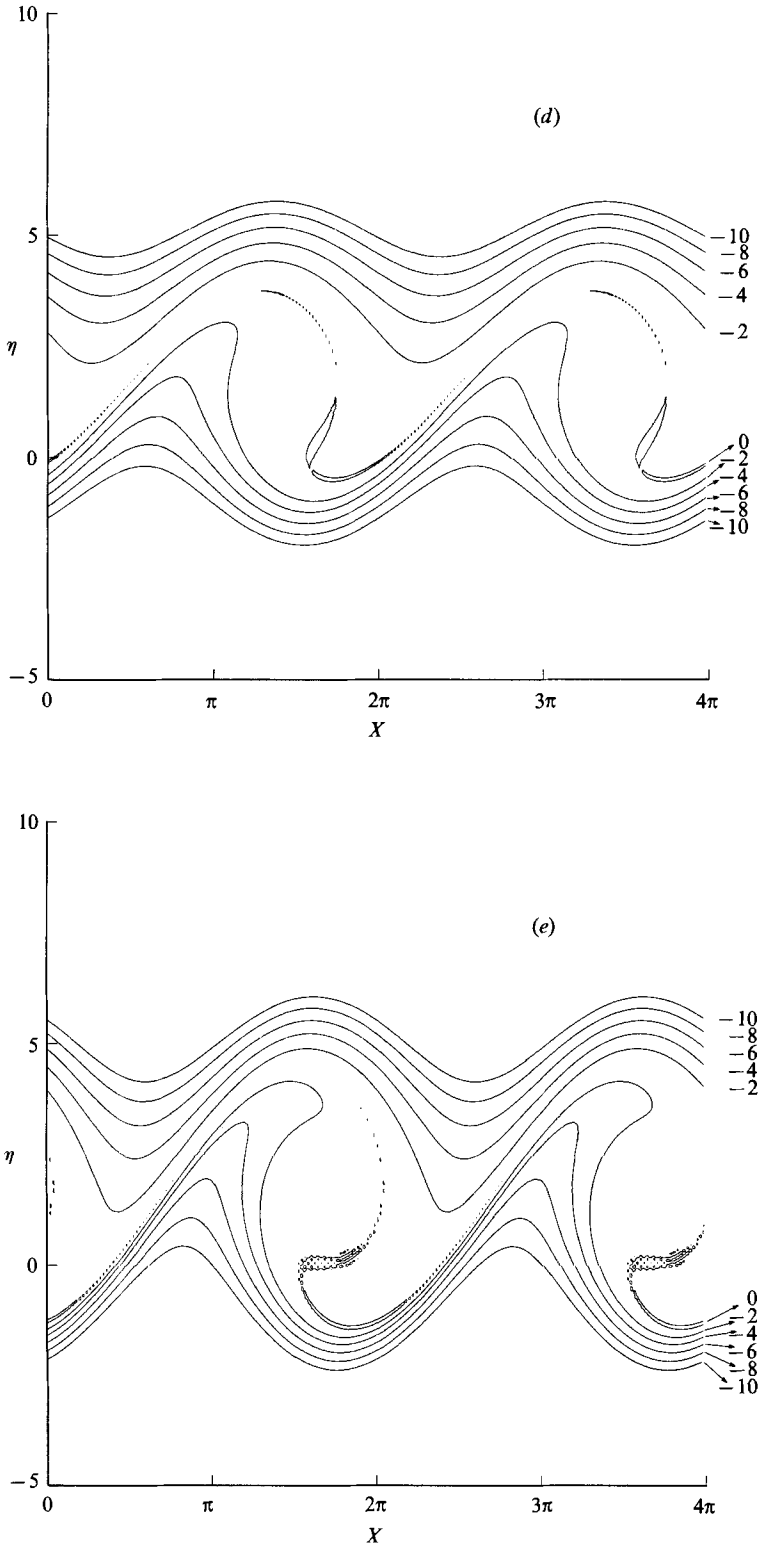

FIGURE 9(*d*, *e*). For caption see page 508.

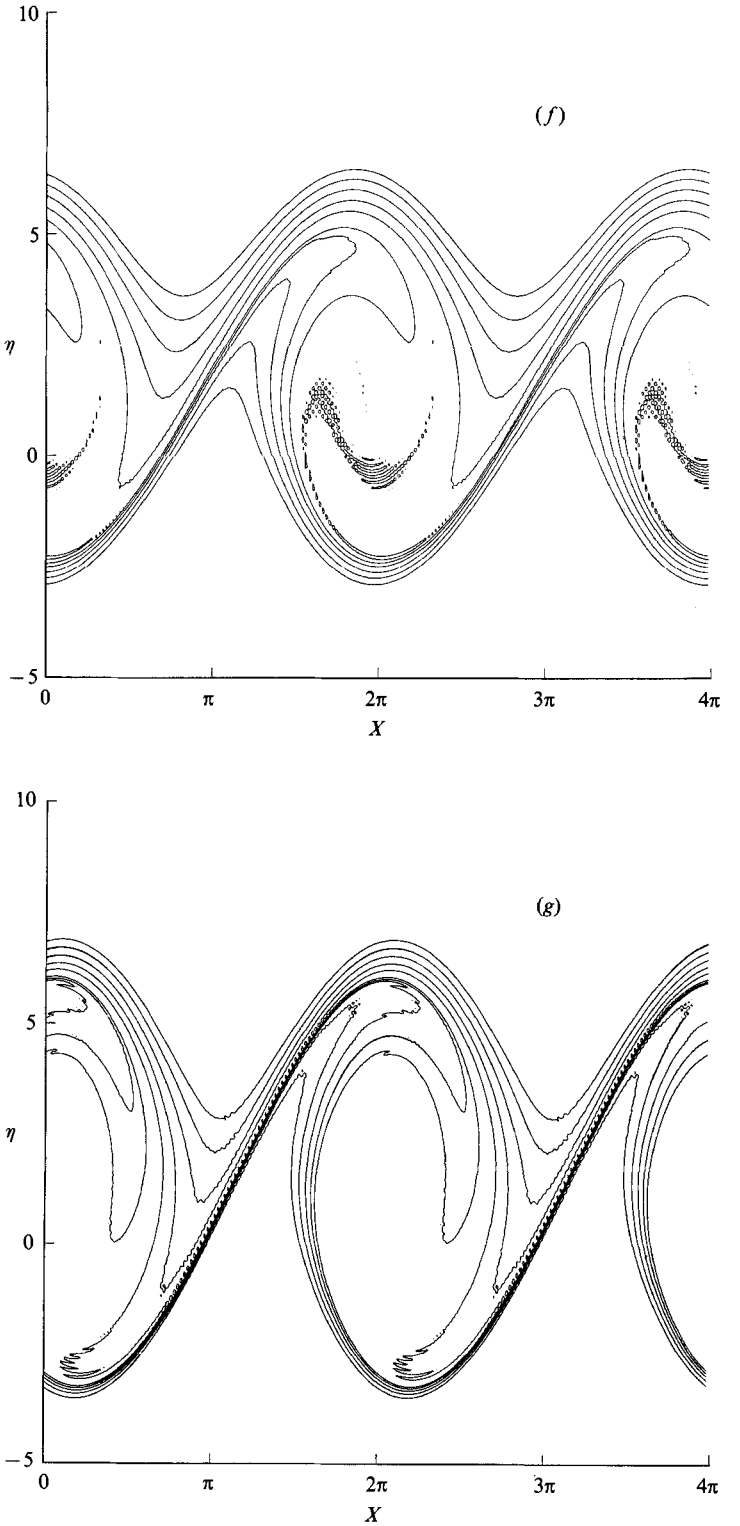

FIGURE 9. Vorticity contours in the $[\eta = -2(Y-S_1)/S_1\bar{U}, X = x-(\bar{U}+\epsilon^{\frac{1}{2}}S_1)t-X_0]$-plane; $\bar{U} = 1.0$. (*a*) $\bar{x} = -3.0$; (*b*) -1.0; (*c*) 0; (*d*) 1.0; (*e*) 1.5; (*f*) 2.0; (*g*) 2.5.

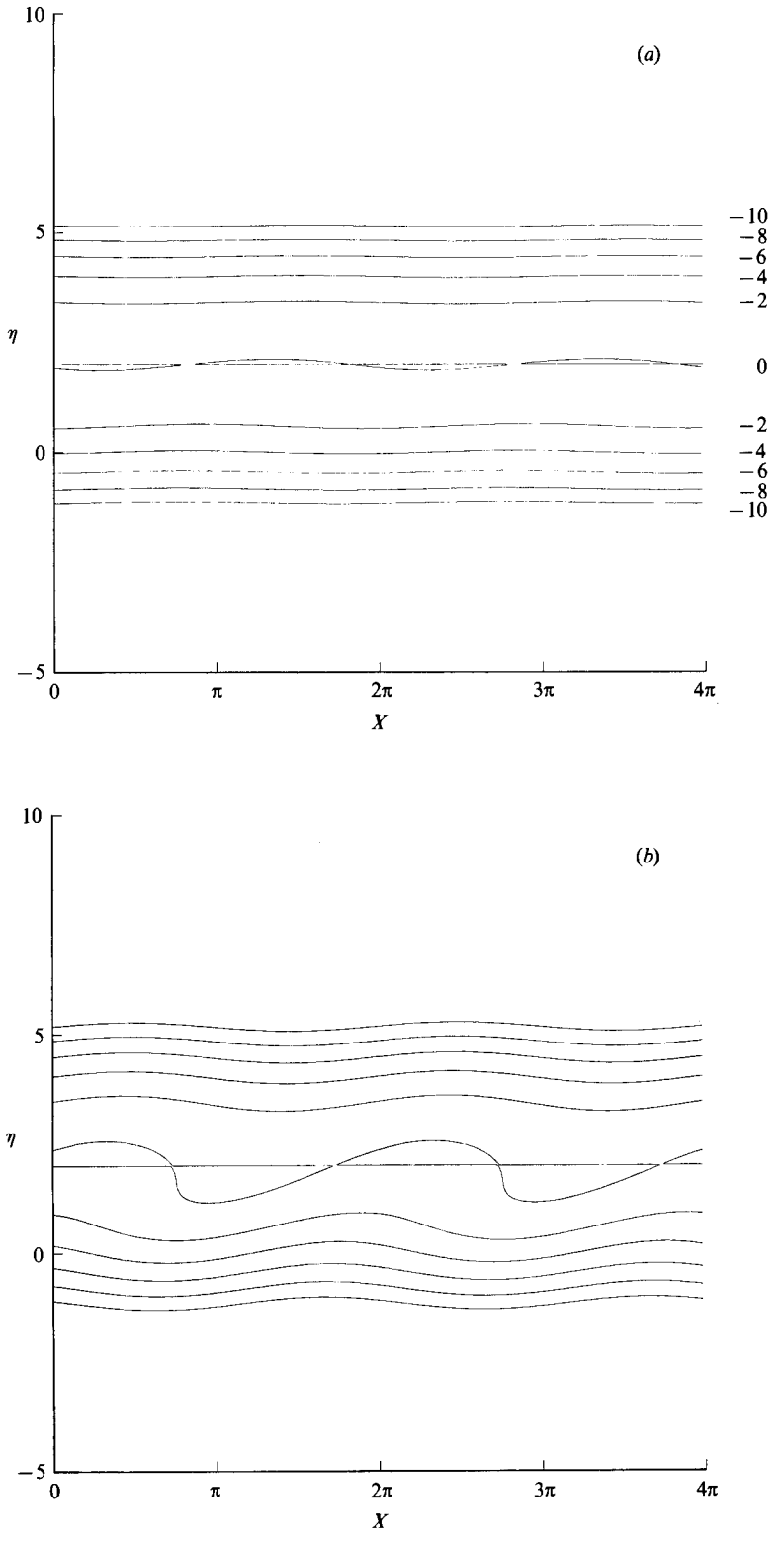

FIGURE 10(*a*, *b*). For caption see next page.

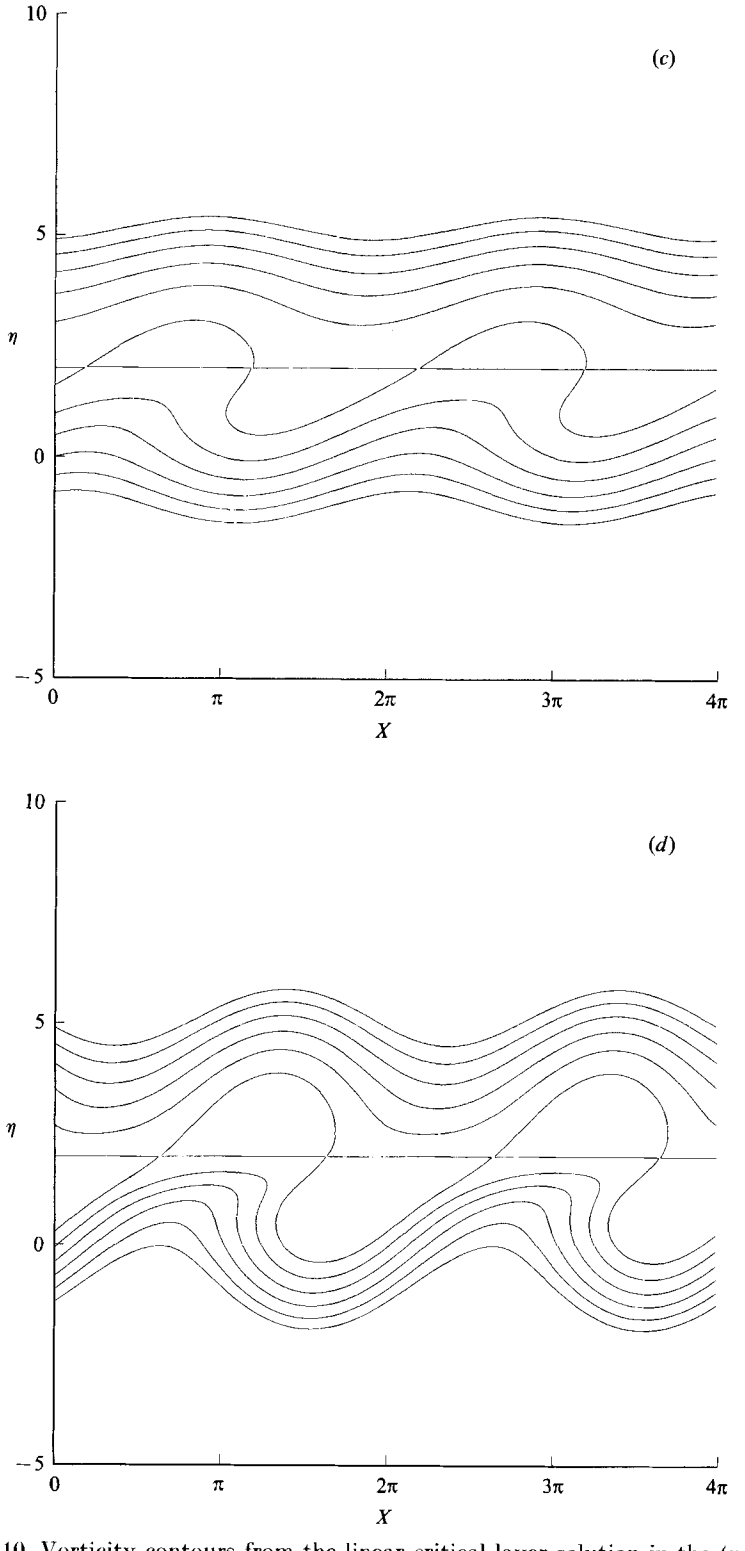

FIGURE 10. Vorticity contours from the linear critical-layer solution in the (η, X)-plane; $\bar{U} = 1.0$. (*a*) $\bar{x} = -3.0$; (*b*) -1.0; (*c*) 0; (*d*) 1.0.

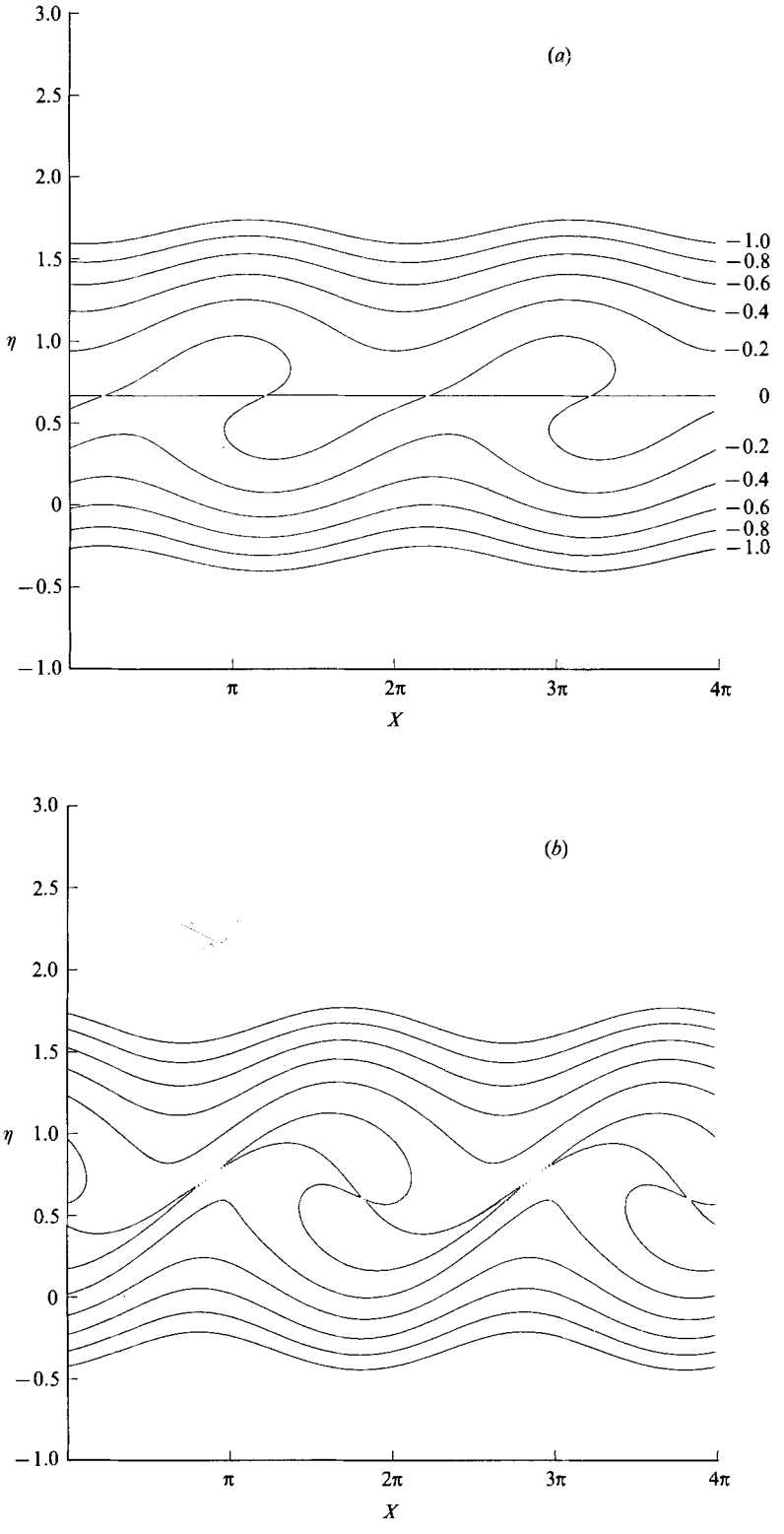

FIGURE 11(*a*, *b*). For caption see page 513.

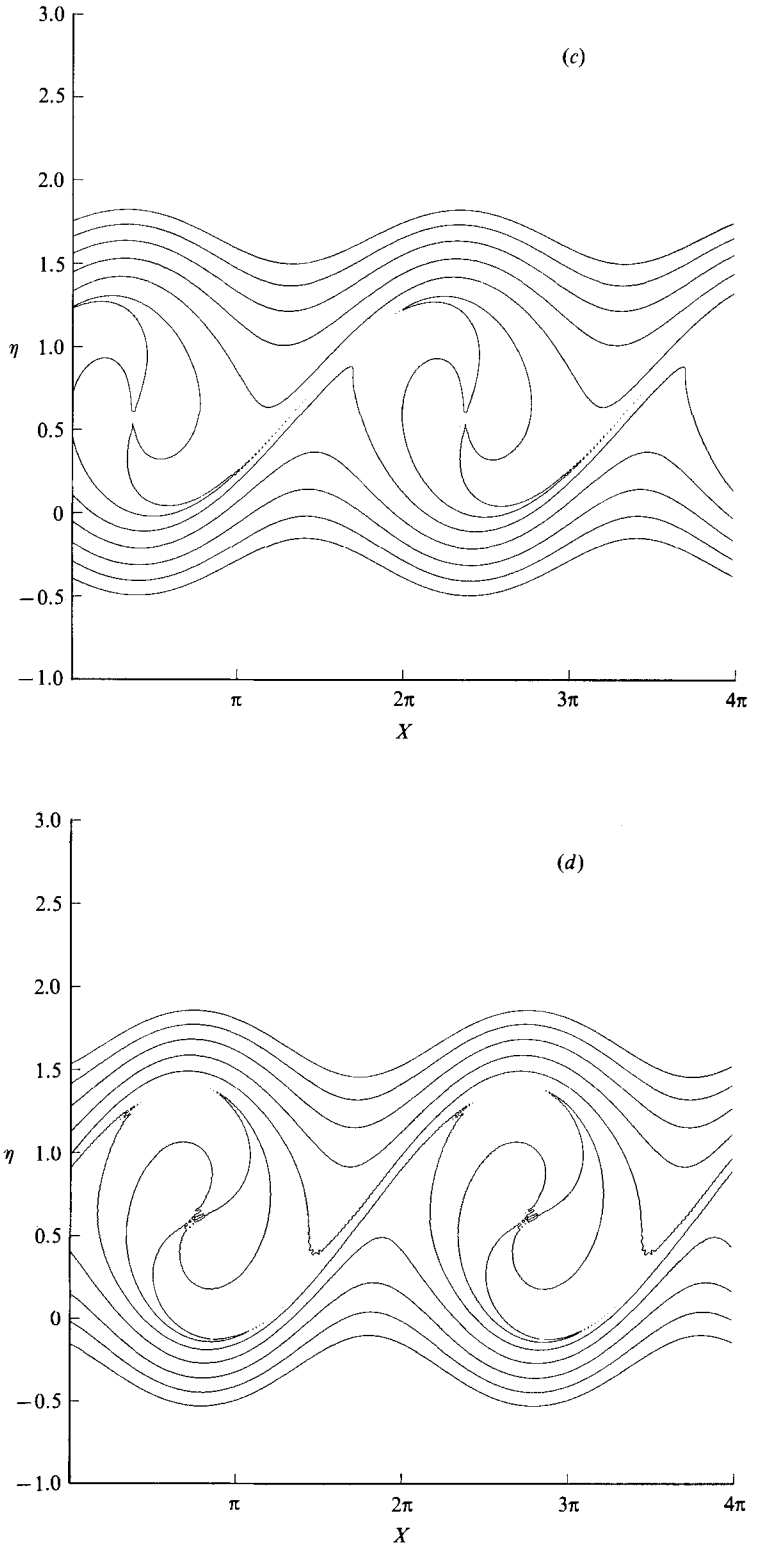

FIGURE 11 (*c*, *d*). For caption see facing page.

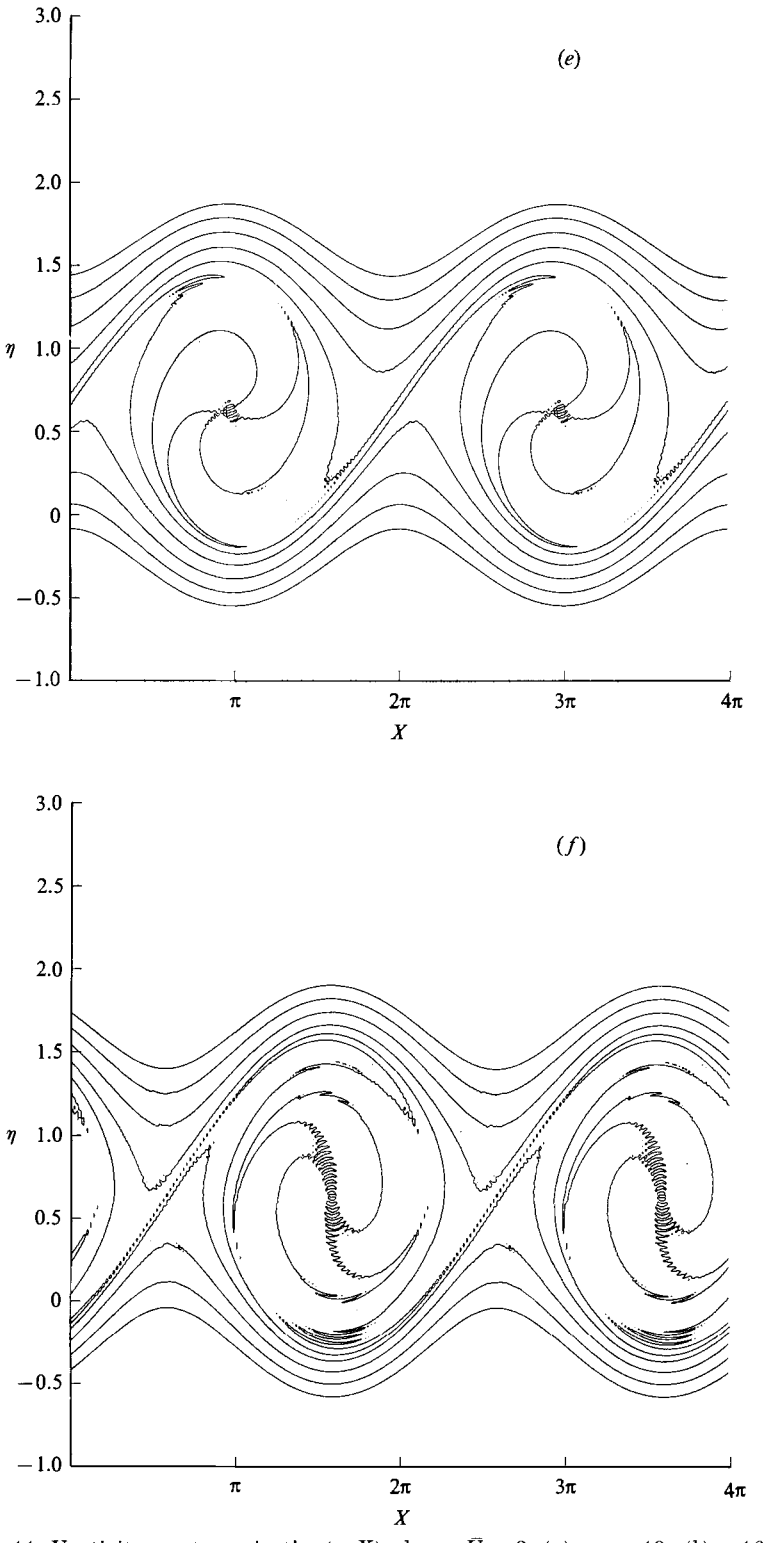

FIGURE 11. Vorticity contours in the (η, X)-plane; $\bar{U} = 3$. (*a*) $\bar{x} = -19$; (*b*) -16; (*c*) -13; (*d*) -11; (*e*) -10; (*f*) -7.

but the subsequent roll-up is not. This is, of course, to be expected, because the linear theory is invalid when the slope of the constant vorticity lines is large.

Figure 11 shows the nonlinear roll-up for the case where $\bar{U} = 3$. It is somewhat similar to the roll-up shown in figure 9, but takes place more gradually. Notice that the lateral extent of the disturbed contours is smaller in this case. Also, the $\Omega_0 = 0$ contour appears to behave somewhat differently in the two cases.

The authors would like to thank Dr S. J. Cowley of Imperial College for his helpful suggestion about the connection with the Stewartson and Warn & Warn solution, Drs L. S. Hultgren and P. A. Durbin for suggesting improvements in the manuscript and the numerical procedures and Bruce Auer and Professor D. B. Taulbee for solving the characteristic equations for comparison with our results.

Appendix

The inhomogeneous term on the right-hand side of (3.27) is

$$\begin{aligned}
F_2^{(1)} = {} & 2\{\operatorname{sech}^3 y \coth y - (y \operatorname{sech} y + \sinh y) \ln|\tanh y| \\
& + \operatorname{sech} y \chi_2(\tanh y)\}\left(\bar{U}\frac{\mathrm{d}}{\mathrm{d}x_1} - \mathrm{i}S_1\right)\frac{\mathrm{d}A^\dagger}{\mathrm{d}x_1} - \operatorname{sech} y(1 + 2\sinh^2 y)\frac{\mathrm{d}^2 A^\dagger}{\mathrm{d}x_1^2} \\
& + 2\operatorname{sech}^2 y \coth y\{\operatorname{sech} y \coth y - (y \operatorname{sech} y + \sinh y) \ln|\tanh y| \\
& + \operatorname{sech} y \chi_2(\tanh y)\}\left(\bar{U}\frac{\mathrm{d}}{\mathrm{d}x_1} - \mathrm{i}S_1\right)^2 A^\dagger - 2\operatorname{sech} y \tanh y\left(\bar{U}\frac{\mathrm{d}}{\mathrm{d}x_1} - \mathrm{i}S_1\right) \\
& \times \frac{\mathrm{d}A^\dagger}{\mathrm{d}x_1} - 2\mathrm{i}\left[\operatorname{sech} y \frac{\mathrm{d}}{\mathrm{d}x_1} a_{\frac{3}{2}}^{(1)\pm} + (y \operatorname{sech} y + \sinh y)\frac{\mathrm{d}}{\mathrm{d}x_1} b_{\frac{3}{2}}^{(1)\pm}\right] \\
& - 2\mathrm{i} \operatorname{sech}^2 y \coth y\left[\operatorname{sech} y\left(\bar{U}\frac{\mathrm{d}}{\mathrm{d}x_1} - \mathrm{i}S_1\right)a_{\frac{3}{2}}^{(1)\pm}\right. \\
& \left. + (y \operatorname{sech} y + \sinh y)\left(\bar{U}\frac{\mathrm{d}}{\mathrm{d}x_1} - \mathrm{i}S_1\right)b_{\frac{3}{2}}^{(1)\pm}\right]. \qquad \text{(A 1)}
\end{aligned}$$

REFERENCES

BENNEY, D. J. & BERGERON, R. F. 1969 A new class of non-linear waves in parallel flows. *Stud. Appl. Maths* **48**, 181–204.

BENNEY, D. J. & MASLOWE, S. A. 1975 The evolution in space and time of nonlinear waves in parallel shear flows. *Stud. Appl. Maths* **54**, 181–205.

BROWAND, F. K. & HO, C. M. 1983 The mixing layer: an example of quasi two-dimensional turbulence. *J. Méc. Théor. Appl.* **2**, 99–120.

CORCOS, G. M. & SHERMAN, F. S. 1976 Vorticity concentration and the dynamics of unstable free-shear layers. *J. Fluid Mech.* **73**, 241–264.

COHEN, J. 1985 Instabilities and resonances in turbulent free shear flows. Ph.D. thesis, University of Arizona.

CRIGHTON, D. G. & GASTER, M. 1976 Stability of slowly diverging jet flow. *J. Fluid Mech.* **77**, 397–413.

DAVIS, R. E. 1969 On high Reynolds number flow over a wavy boundary. *J. Fluid Mech.* **36**, 337–346.

GASTER, M., KIT, E. & WYGNANSKI, I. 1985 Large-scale structures in a forced turbulent mixing layer. *J. Fluid Mech.* **150**, 23–39.

GOLDSTEIN, M. E., DURBIN, P. A. & LEIB, S. J. 1987 Roll-up of vorticity in adverse-pressure-gradient boundary layers. *J. Fluid Mech.* **183**, 325–342.

HABERMAN, R. 1972 Critical layers in parallel shear flows. *Stud. Appl. Maths* **51**, 139–161.

HAYNES, P. H. 1985 Nonlinear instability of a Rossby-wave critical layer. *J. Fluid Mech.* **161**, 493–511.

HICKERNELL, F. J. 1984 Time-dependent critical layers in shear flows on the beta-plane. *J. Fluid Mech.* **142**, 431–449.

HO, C.-M. & HUANG, L.-S. 1982 Subharmonics and vortex merging in mixing layers. *J. Fluid Mech.* **119**, 443–473.

HO, C. M. & HUERRE, P. 1984 Perturbed free shear layers. *Ann. Rev. Fluid Mech.* **16**, 365–424.

HUERRE, P. 1977 Nonlinear instability of free shear layers. In *Laminar–Turbulent Transition, AGARD CP*, pp. 224–229.

HUERRE, P. 1980 The nonlinear stability of a free shear layer in the viscous critical layer regime. *Phil. Trans. R. Soc. Lond.* A **293**, 643–672.

HUERRE, P. 1987 On the Landau constant in mixing layers. *Proc. R. Soc. Lond.* A **409**, 369–381.

HUERRE, P. & SCOTT, J. F. 1980 Effects of critical layer structure on the nonlinear evolution of waves in free shear layers. *Proc. R. Soc. Lond.* A **371**, 509–524.

JAMES, M. L., SMITH, G. M. & WOLFORD, J. C. 1977 *Applied Numerical Methods for Digital Computation.* Harper and Row.

KILLWORTH, P. D. & MCINTYRE, M. E. 1985 Do Rossby-wave critical layers absorb, reflect, or over-reflect? *J. Fluid Mech.* **161**, 449–492.

MASLOWE, S. 1986 Critical layers in shear flows. *Ann. Rev. Fluid Mech.* **18**, 405–432.

MICHALKE, A. 1964 On the inviscid instability of the hyperbolic-tangent velocity profile. *J. Fluid Mech.* **19**, 543–556.

MIURA, A. & SATO, T. 1978 Theory of vortex nutation and amplitude oscillation in an inviscid shear instability. *J. Fluid Mech.* **86**, 33–47.

MONKEWITZ, P. A. & HUERRE, P. 1982 The influence of the velocity ratio on the spatial instability of mixing layers. *Phys. Fluids* **25**, 1137–43.

OSTER, D. & WYGNANSKI, I. 1982 The forced mixing layer between parallel streams. *J. Fluid Mech.* **123**, 91–130.

PLASCHKO, P. & HUSSAIN, A. K. M. F. 1984 A spectral theory for weakly nonlinear instabilities of slowly divergent shear flows. *Phys. Fluids* **27**, 1603–1606.

ROBINSON, J. L. 1974 The inviscid nonlinear instability of parallel shear flows. *J. Fluid Mech.* **63**, 723–752.

RU-SUE KO, D., KOBATA, T. & LEES, L. 1970 Finite disturbance effect on the stability of a laminar incompressible wake behind a flat plate. *J. Fluid Mech.* **40**, 315–341.

STEWARTSON, K. 1978 The evolution of the critical layer of a Rossby wave. *Geophys. Astrophys. Fluid Dyn.* **9**, 185–200.

STEWARTSON, K. 1981 Marginally stable inviscid flows with critical layer. *IMA J. Appl. Maths* **27**, 133–175.

STUART, J. T. 1960 On the non-linear mechanics of wave disturbances in stable and unstable parallel flows. Part 1. *J. Fluid Mech.* **9**, 353–370.

VAN DYKE, M. D. 1975 *Perturbation Methods in Fluid Mechanics.* Parabolic.

WARN, T. & WARN, H. 1978 The evolution of a nonlinear critical level. *Stud. Appl. Maths* **59**, 37–71.

WATSON, J. 1960 On the non-linear mechanics of wave disturbances in stable and unstable parallel flows. Part 2. *J. Fluid Mech.* **9**, 371–389.

WYGNANSKI, I. J. & PETERSEN, R. A. 1987 Coherent motion in excited free shear flows. *AIAA J.* **25**, 201–212.